

1 **A new model for the global biogeochemical cycle of carbonyl**
2 **sulfide. Part 1: Assessment of direct marine emissions with an**
3 **oceanic general circulation and biogeochemistry model**

4

5 **T. Launois¹, S. Belviso¹, L. Bopp¹, C.G. Fichot² and P. Peylin¹**

6 [1] Laboratoire des Sciences du Climat et de l'Environnement (LSCE Saclay), IPSL, CEA,
7 CNRS, UVSQ, CE Saclay, Bât 703 L'Orme des Merisiers, 91191, Gif-sur-Yvette, France

8 [2] Jet Propulsion Laboratory, California Institute of Technology, Pasadena, California, USA

9

10 Correspondence to: T. Launois (thomas.launois@lsce.ipsl.fr)

11

12 **Abstract**

13 The global budget of tropospheric carbonyl sulfide (OCS) is believed to be at equilibrium
14 because background air concentrations have remained roughly stable over at least the last
15 decade. Since the uptake of OCS by leaves (associated to photosynthesis) and soils have been
16 revised significantly upwards recently, an equilibrated budget can only be obtained with a
17 compensatory source of OCS. It has been assumed that the missing source of OCS comes
18 from the low-latitude ocean, following the incident solar flux. The present work uses
19 parameterizations of major production and removal processes of organic compounds
20 in the NEMO-PISCES Ocean General Circulation and Biogeochemistry Model to assess the
21 marine source of OCS. In addition, the OCS photo-production rates computed
22 with the NEMO-PISCES model were evaluated independently using the UV absorption
23 coefficient of chromophoric dissolved organic matter (derived from satellite ocean color) and
24 apparent quantum yields available in the literature. Our simulations show global direct marine
25 emissions of OCS in the range of 573-3997 GgS yr⁻¹, depending mostly on the quantification
26 of the absorption rate of chromophoric dissolved organic matter. The high estimates on that
27 range are unlikely, as they correspond to a formulation that most likely overestimate photo-
28 production process. Low and medium (813 GgS yr⁻¹) estimates derived from the NEMO-
29 PISCES model are however consistent spatially and temporally with the suggested missing
30 source of Berry et al. (2013), allowing thus to close the global budget of OCS given the recent
31 estimates of leaf and soil OCS uptake.

1 **1 Introduction**

2 Carbonyl sulfide (OCS) is a long-lived sulfur-containing trace gas with direct and indirect
3 effects on the radiation budget of the atmosphere (OCS being both a tropospheric greenhouse
4 gas and a source of sulfur aerosols to the stratosphere). But these radiative effects are low
5 compared to the radiative forcings of greenhouse gases (GHG) and tropospheric aerosols of
6 anthropogenic origin (Brühl et al., 2012 and references therein). But because OCS is the most
7 abundant sulfur-containing gas in the atmosphere, it is a major contributor to the stratospheric
8 sulfate layer during volcanically quiescent periods (Notholt et al., 2003). OCS also
9 participates in some key reactions within the global carbon cycle, especially reactions
10 associated with leaf photosynthesis and soil microbial activities (Berry et al., 2013 and
11 references therein). As such, it holds great promises for the studies of plant physiology,
12 terrestrial ecosystem production and the global carbon cycle thanks to its potential use as a
13 tracer for canopy photosynthesis, transpiration and stomatal conductance (Wohlfahrt et al.,
14 2012 and references therein).

15 Measurements of OCS from the global air-monitoring network of the National Oceanic and
16 Atmospheric Administration (NOAA) provided compelling evidence for the existence of a
17 major sink of this gas in the continental boundary layer, mainly attributed to biospheric uptake
18 (Montzka et al., 2007; Campbell et al., 2008). The uptake of OCS by plants was modeled to
19 be no more than 240 GgS yr⁻¹ by Kettle et al. (2002), but it has been recently revised upwards,
20 with new estimates of 490 GgS yr⁻¹ (Suntharalingam et al., 2008), of 738 GgS yr⁻¹ in the work
21 of Berry et al. (2013) and even reaching up to 1500 GgS yr⁻¹ in Montzka et al. (2007). Soils
22 could also play a role in the budget of OCS. It is still a strong matter of debate but recent
23 estimates suggest that much more OCS is taken up by soils than proposed by Kettle et al.
24 (2002) (355 GgS yr⁻¹, according to Berry et al., 2013, compared with an estimate of around
25 130 GgS yr⁻¹ in Kettle et al., 2002). Since background air concentrations have remained
26 roughly stable over at least the last decade (Montzka et al., 2007), the global budget of
27 tropospheric OCS is believed to be at equilibrium. Kettle et al. (2002) proposed a global
28 budget of OCS with ocean and anthropogenic sources compensating for the main uptake by
29 vegetation. However, because deposition fluxes of OCS to vegetation and soils are three times
30 higher than proposed in the study by Kettle et al. (2002), an equilibrated budget can only be
31 obtained with a compensatory source of OCS. Berry et al. (2013) suggests that the missing
32 source of OCS comes from the oceans. This missing source has been inferred through a
33 simple inversion approach that optimizes sources and sinks based on global measurements of

1 atmospheric OCS mixing ratios collected in the NOAA network. This inversion pointed
2 towards a larger global oceanic source of OCS with higher proportions of tropical emissions
3 than previously established.

4 The ocean is believed to be the largest source of atmospheric OCS (Chin and Davis, 1993;
5 Kettle et al., 2002; Berry et al., 2013). It contributes to OCS in the troposphere by direct
6 emission of this gas, and by large emissions of carbon disulfide (CS₂) and dimethylsulfide
7 (DMS) quickly oxidized into OCS (with an approximate lifetime of 1 day) (Barnes et al.,
8 1994; Kloster, 2006). Barnes et al. (1994) suggested that OCS accounts for 0.7% of the
9 oxidation products of DMS, and that 87% of the marine emissions of CS₂ are converted into
10 OCS. However, estimates of sea-air fluxes of OCS and their spatial distributions remain
11 largely unknown. Kettle et al. (2002) simulated direct global oceanic OCS fluxes from -110
12 GgS yr⁻¹ (a sink) to 190 GgS yr⁻¹ (a source to the atmosphere), while previous estimates based
13 on field observations suggested global direct oceanic OCS emissions from 160 to 640 GgS yr⁻¹
14 (Chin and Davis, 1993; Watts, 2000). The Kettle et al. (2002) study suggested that direct
15 sea-air OCS emissions mainly take place at mid and high latitudes, during the respective
16 periods of maximum irradiance.

17 OCS surface concentrations show a strong diurnal cycle with a mid-afternoon maximum,
18 suggesting that photo-production is a major source of marine OCS (Ferek and Andreae, 1984;
19 Xu et al., 2001; Von Hobe et al., 2003). In addition, OCS can also be produced in marine
20 waters when no light is available. This pathway is therefore called dark-production.
21 Measurements by Von Hobe et al. (2001) indicated that its rate is proportional to the amount
22 of organic material, and it has therefore so far been linked to the chromophoric dissolved
23 organic matter (CDOM) absorption coefficient (Von Hobe et al., 2001 and 2003). Finally,
24 OCS surface concentrations and fluxes are also strongly influenced by the continuous
25 temperature- and pH-dependent hydrolysis of OCS to carbon dioxide (CO₂) and hydrogen
26 sulfide (H₂S) (Von Hobe et al., 2003).

27 The present work reassesses the marine source of OCS using the 3D oceanic NEMO-PISCES
28 Ocean General Circulation and Biogeochemistry model with process-based parameterizations
29 of the main OCS production and removal processes (Fig. 1). The present study proposes two
30 independent approaches to quantify the photo-production of OCS. The dark-production rate
31 implemented in the NEMO-PISCES model follows the formulation of Von Hobe et al. (2001,
32 2003). Therefore, the dark-production rate, even if supposed to be light-independent, is also
33 linked to the chromophoric dissolved organic matter absorption coefficient at 350nm (a_{350}), as

1 the variable provides an indirect estimate of the seawater richness in organic matter. As
2 parameterizations found in literature for both dark- and photo-production of OCS are related
3 to the UV absorption coefficient of CDOM at 350 nm, sensitivity tests are performed using
4 three different formulations for this variable. Sensitivity tests are also performed on
5 hydrolysis, exploring two different formulations. Global maps of OCS concentrations
6 obtained with the NEMO-PISCES model are compared with in-situ measurements. Finally,
7 the magnitude and spatial distributions of global OCS emissions modeled in the present work
8 are compared to previous global estimates.

10 **2 Methods**

11 **2.1 Description of NEMO-PISCES and experimental design**

12 In this study, we use the Pelagic Interaction Scheme for Carbon and Ecosystem Studies
13 (PISCES) ocean biogeochemical model. As a detailed description of the model
14 parameterizations is given in Aumont and Bopp (2006), the model is only briefly presented
15 here. The model has 24 compartments, including four living pools: two phytoplankton size
16 classes/groups (nanophytoplankton and diatoms) and two zooplankton size classes
17 (microzooplankton and mesozooplankton). Phytoplankton growth can be limited by five
18 different nutrients: nitrate, ammonium, phosphate, silicate and iron. The internal
19 concentrations of chlorophyll for both phytoplankton groups are prognostically simulated
20 with Chlorophyll-to-Carbon ratios computed as a function of light and nutrient stress. There
21 are three nonliving compartments: semi-labile dissolved organic matter (with remineralization
22 timescales of several weeks to several years), small and large sinking particles. In addition to
23 the version of the model used in Aumont and Bopp (2006), we also include here a prognostic
24 module computing OCS concentrations in seawater.

25 PISCES is coupled to the general circulation model Nucleus for European Modelling of the
26 Ocean (NEMO, Madec et al. 1998). A release of the model is available for the community
27 (<http://www.nemo-ocean.eu/>). Here, we use the global configuration ORCA2 with a
28 resolution of $2^\circ \times 0.5\text{-}2^\circ$ and 31 vertical levels (with a $\sim 10\text{m}$ -resolution in the first 200m).
29 NEMO-PISCES is first run 3,000 years to obtain an equilibrated state, forced in offline mode
30 by the Consortium for Oceanic Research and Education (CORE2) Normal Year Forcing,
31 (Large and Yeager (2008)) and initialized with climatological nutrient data. The OCS module
32 is then only run two additional years as it converges towards equilibrium much more rapidly.
33 The results presented in this study correspond to the last year of this simulation.

2.2 Parameterizations of OCS production and removal processes implemented in NEMO-PISCES

The clear diurnal cycle of sea-surface OCS concentrations with peak values during mid-afternoon suggests photochemical processes play an important role in the production of OCS. Organo-sulfur compounds with thiol groups (-SH), such as cysteine and methyl mercaptans (CH₃SH), have been suggested as OCS precursors (Ferek and Andreae, 1984; Flöck et al., 1997; Ulshöfer et al., 1996). Moreover, measured CH₃SH diurnal cycles were coherent with the hypothesis that its photo-destruction could lead to OCS production (Xu et al., 2001). Because no global map of CH₃SH is available, we followed parameterizations of OCS photo-production found in literature which relate photo-production rate of OCS to the UV irradiance intensity at the sea surface and to the efficiency of chromophoric dissolved organic matter (CDOM) available to absorb this UV radiation. The quantification of this photochemical process can be amenable to remote sensing because of its critical dependence on ocean UV and visible optical properties. Additional parameterizations were needed to complete the description of OCS formation and destruction processes in NEMO-PISCES. We therefore implemented specific equations to calculate the formation of OCS via dark-production (a light-independent pathway) and the hydrolysis rate of OCS in sea waters. Finally, air-sea exchanges of OCS were described in an analogous way to Fick's diffusion law.

2.2.1 UV light penetration in seawater:

In NEMO-PISCES, surface irradiance received at each grid point is a function of cloud coverage and deduced surface UV irradiance is taken equal to 4.4% of the total light received at sea surface. UV penetration at depth in marine waters in NEMO-PISCES was taken equal to the penetration calculated with the deep blue wavelength for visible light attenuation coefficient. As this is a rough approximation and might lead to over-estimating maximum depth penetration for UV irradiance, we set the UV value to zero for layers deeper than 30 m, which corresponds to the average depth at which less than 10% of surface UV irradiance penetrates for marine waters containing less than 1 mg m⁻³ of chlorophyll (Bricaud et al., 1995; Tedetti et al., 2007).

2.2.2 Parameterization of CDOM absorption coefficient at 350 nm (a_{350})

Chromophoric (or colored) dissolved organic matter (CDOM) is the fraction of the dissolved organic matter that absorbs light, ranging from ultraviolet to visible wavelengths. CDOM has been identified as one of the most influential factor to control UV attenuation in waters. Its concentration increases in seawater with elevated biological production rates and terrestrial

1 inputs. CDOM distribution is also controlled by the deep ocean circulation, upwelling and/or
2 vertical mixing (Para et al., 2010 and references therein). Its concentration decreases with
3 photochemical degradation and microbial consumption. CDOM absorbs part of available
4 light, therefore negatively impacting primary productivity of aquatic ecosystems. However, as
5 provider of a substitute for microbial respiration, photo-degraded CDOM positively impacts
6 the secondary productivity of the oceanic ecosystems.

7 As no reliable parameterization is currently available to calculate CDOM concentrations, due
8 to insufficient knowledge on the controlling processes of CDOM formation and destruction,
9 we chose to follow the study from Para et al. (2010) and assumed that the CDOM absorption
10 at 350nm (a_{350}) was a good indicator of CDOM concentrations. OCS production pathways are
11 either dependent on irradiances in the UV domain (photo-production) or on CDOM and
12 organic matter concentrations (dark-production). As a_{350} allows a link with both variables, it is
13 a key parameter in our parameterizations of OCS production. Sensitivity tests were performed
14 using NEMO-PISCES and three different formulations of a_{350} .

15 The first two formulations of CDOM absorption coefficients were proposed by Morel and
16 Gentili (2009) and Preiswerk et al. (2000), who deduced them at a given wavelength from in
17 situ measurements, and then extrapolated the absorption coefficient of CDOM at 350 nm by
18 using the following standard exponential relation:

$$19 \quad a_{CDOM}(\lambda) = a_{CDOM}(\text{ref}) * e^{(-S*(\text{ref}-\lambda))} \quad (1)$$

20 where S is the spectral slope coefficient of CDOM between λ and the reference wavelength
21 (ref).

22 **a) a_{350} from Morel and Gentili (2009)**

23 The parameterization of a_{350} from Morel and Gentili (2009) is based on spectral reflectances
24 of the ocean over Case 1 waters. Case 1 waters are those for which the optical properties of
25 CDOM closely follow the optical properties of phytoplankton, as defined in Morel (1988).
26 Spectral reflectances were derived from ocean color remote sensing data at several
27 wavelengths to allow separation between CDOM and chlorophyll reflectance signatures.
28 Products from SeaWiFS monthly global composites for the 2002-2007 period were used, and
29 led to the following relation between CDOM absorption coefficient and chlorophyll
30 concentration:

$$a_{CDOM}(400) = 0.065[\text{Chl}]^{0.63} \quad (2)$$

31 **b) a_{350} from Preiswerk et al. (2000)**

1 The second parameterization was taken from Preiswerk et al. (2000) who deduced a_{350} from
 2 modeled CDOM absorption coefficient at 440 nm. To model a_{440} , satellite ocean color data
 3 were used as a proxy for chlorophyll concentration and combined with the relation of Garver
 4 and Siegel (1998), Eq. (3):

$$5 \quad \text{per}(a_{440}) = -26 [\log(\text{chl})] + 26 \quad (3)$$

$$6 \quad a_{PH,440} = 0.0448\text{chl} \quad (4)$$

$$7 \quad \text{per}(a_{440}) = \frac{a_{440}}{a_{PH,440} + a_{440}} * 100\% \quad (5)$$

8 where $a_{PH,440}$ is the absorption coefficient of the phytoplankton at 440 nm, and $\text{per}(a_{440})$ is
 9 the percent of the total non-seawater absorption coefficient at 440 nm (due to CDOM).

Deleted: 26

10 c) a_{350} from MODIS *Aqua* ocean color

11 A relationship between a_{350} and chlorophyll-a was established independently, using MODIS
 12 *Aqua* ocean color data collected continuously between July 2002 and July 2010. Monthly
 13 climatologies of MODIS *Aqua* chlorophyll-a surface concentrations were used, and MODIS
 14 *Aqua* remote-sensing reflectances were used to derive corresponding monthly climatologies
 15 of a_{350} for the global surface ocean. The SeaUV algorithm developed by Fichot et al. (2008)
 16 was used to estimate the diffuse attenuation coefficient at 320 nm, $K_d(320)$, from the remote-
 17 sensing reflectances. A ratio $a_{CDOM}(320)/K_d(320) = 0.68$ derived from an extensive set of in
 18 situ measurements was then used to calculate the absorption coefficient of CDOM at 320 nm,
 19 a_{320} , from $K_d(320)$ (Fichot and Miller, 2010). A spectral slope coefficient of 0.0198 derived
 20 from the same *in situ* data set was then used to calculate a_{350} from a_{320} using Eq. (1).

21 The a_{350} data from the twelve monthly climatologies were regressed on the corresponding
 22 MODIS *Aqua* chlorophyll-a concentrations using the fourth-order polynomial shown in Eq.
 23 (6).

$$24 \quad \ln(a_{350}) = 0.5346C - 0.0263C^2 - 0.0036C^3 + 0.0012C^4 - 1.6340 \quad (6)$$

25 where $[Chl]$ has units of mg m^{-3} , and a_{350} has units of m^{-1} .

Deleted: = ln([Chl]), and [

26 The equation 6 was then added in NEMO-PISCES to complete the sensitivity tests of the
 27 OCS concentrations on the different a_{350} expressions tested.

28 2.2.3 OCS photo-production rates as modeled in NEMO-PISCES

29 OCS photo-production is primarily induced by the interaction of UV radiation and natural
 30 photosensitizers in CDOM (Ferek and Andreae, 1984; Flöck et al., 1997). Therefore, Uher et
 31 al. (1997) photo-production parameterization takes into account both the incident UV
 32 irradiance and OCS production efficiency (apparent quantum yield, AQY). An AQY

1 represents the spectral efficiency of a photochemical process (e.g., photochemical production
2 of OCS), and is generally determined in the laboratory by normalizing the quantity of OCS
3 produced during solar exposure to the amount of photons absorbed by CDOM during that
4 same solar exposure. The resulting expression for photoproduction rate proposed is:

$$5 \quad P = p UV \quad (7a)$$

6 where P is the OCS photo-production rate, p a zeroth-order photoproduction constant (fmol L^{-1}
7 $\text{s}^{-1} \text{W}^{-1} \text{m}^2$) and UV the solar UV light density.

8 This expression was established using strong assumptions, such as considering that no other
9 source or sink of OCS affects OCS concentration in seawaters. The authors found mean
10 values for the photoproduction constant around $1.3 \pm 0.3 \text{ fmol L}^{-1} \text{ s}^{-1} \text{ W}^{-1} \text{ m}^2$ on offshore
11 samples and values twice as high in inshore waters.

12 A few AQY for OCS have been published, but they exhibit considerable variability, with
13 values varying by a factor of >7 depending on the environment considered (quantum yields
14 ranging from $9.3 \cdot 10^{-8}$ to $6.4 \cdot 10^{-7}$ in the Sargasso Sea for Weiss et al., 1995a and Zepp et al.,
15 1994, respectively). The quantum yields depend both on the location and the season of the
16 measurement, especially because CDOM quality and its absorption coefficient might vary
17 through time (Kettle et al., 2002; Weiss, 1995b; Cutter et al., 2004). To compensate for part of
18 this natural variability, Uher et al. (1997) normalized the measured AQY by the absorption
19 coefficient of CDOM available for the reaction at the same location. Therefore, the new
20 relation, implemented in NEMO-PISCES, is the following:

$$21 \quad P = a_{350} UV \frac{p}{a_{350}} = k a_{350} UV \quad (7b)$$

22 where P is the OCS photo-production rate ($\text{pmol m}^{-3} \text{ s}^{-1}$), UV is the incident irradiance
23 integrated from 295 to 385nm (W m^{-2}). The k coefficient is retrieved from the normalization
24 of measured photoproduction constants to measured CDOM absorption coefficient values at
25 350 nm. For offshore waters (the majority of globe waters), k was found to be close to a value
26 of $2.1 \text{ fmol L}^{-1} \text{ s}^{-1} \text{ W}^{-1} \text{ m}^3$. Note that the k coefficient deduced from inshore water samples
27 was found to be $2.8 \text{ fmol L}^{-1} \text{ s}^{-1} \text{ W}^{-1} \text{ m}^3$ on average. The smaller difference between the two k
28 values justified the choice to use this normalized expression rather than Eq. 8a which showed
29 more sample-dependence.

30 **2.2.4 Parameterization of OCS dark-production rates**

31 Measurements of large OCS concentrations well below the photic zones have proven that
32 OCS can be produced when no light is available. The so-called dark-production pathway was
33 shown to largely depend on available organic matter. The pool of organic matter is quantified

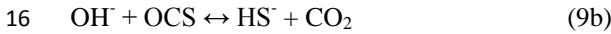
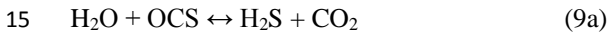
1 by the a_{350} parameter, following Para et al. (2010), as explained in Section 2.2.2. Microbial
 2 activities are suggested as main precursors for the OCS dark-production pathway, but their
 3 exact nature and the mechanisms underlying this process are poorly known. Von Hobe et al.
 4 (2001, 2003) calculated dark-production rates assuming that after dawn OCS concentrations
 5 were reaching a steady-state when dark-production was compensating for the parallel
 6 hydrolysis. Equation 8 was established using measurements from a campaign in the Sargasso
 7 Sea and hydrolysis rates were calculated following the Elliott et al. formulation (1989).
 8 The formulation from Von Hobe et al. (2001) relating OCS dark-production rates to the
 9 CDOM absorption coefficient was implemented in NEMO-PISCES following:

$$10 \quad Q = a_{350} e^{(55.8 - \frac{16200}{T})} \quad (T \text{ in K}) \quad (8)$$

11 where Q is the dark-production rate in $\text{pmol m}^{-3} \text{ s}^{-1}$, and a_{350} is the CDOM absorption
 12 coefficient which is used here to describe the CDOM/organic matter concentration.

13 **2.2.5 Hydrolysis of OCS**

14 OCS is chemically removed in seawater through reaction with H_2O and OH^- :



17 OCS hydrolysis rate measurements were done in the dark, using filtered water, therefore
 18 cancelling the potential impact of parallel dark-production. Reactions 10a and 10b are actually
 19 composites of complex mechanisms involving several intermediates, and concentrations that
 20 have been used to calculate hydrolysis rates are much larger than observed in seawater, which
 21 may lead to some errors.

22 We performed sensitivity tests in NEMO-PISCES by using two different hydrolysis
 23 parameterizations to study the impact of the choice of the hydrolysis constant formulation.

24 Both Kamyshny et al. (2003) and Elliott et al. (1989) relate the value of OCS hydrolysis
 25 constant to the marine water pH and its temperature, following respectively:

$$26 \quad k_{hydr_Elliott} = e^{(24.3 - \frac{10450}{T})} + \frac{k_w}{[H^+]} e^{(22.8 - \frac{6040}{T})} \quad (T \text{ in K}) \quad (10a)$$

$$27 \quad k_{hydr_Kamyshny} = 4.19E^{-12} e^{(-\frac{12110}{T})} + \frac{k_w}{[OH^-]} 1.41E^{18} e^{(-\frac{11580}{T})} \quad (T \text{ in K}) \quad (10b)$$

28

29 With k_w the ion product of marine water, $[OH^-]$ and $[H^+]$ the OH^- and H^+ activities.

30 Both hydrolysis constant rates, as function of temperature, are represented in the case of
 31 $\text{pH}=8.2$ in Fig. 2.

32 **2.2.6 OCS sea-to-air fluxes**

1 OCS exchange between the ocean and the atmosphere can be described in an analogous way
 2 to Fick's diffusion law. The sea-air OCS flux depends on the OCS concentration in sea water
 3 and the partial pressure of OCS in air:

$$4 \quad F_{OCS} = k_{water} \left([OCS]_{aq} - \frac{[OCS]_{atm}}{H} \right) \quad (11)$$

5 where F_{OCS} is the sea-air flux ($\text{pmol m}^{-2} \text{s}^{-1}$), $[OCS]_{aq}$ and $[OCS]_{atm}$ are the OCS concentration
 6 at sea surface and in the atmosphere respectively (in pmol m^{-3}). The atmospheric OCS
 7 concentration $[OCS]_{atm}$ over sea surface was constantly imposed when running NEMO-
 8 PISCES, assuming an atmospheric mixing ratio of 500 ppt. Through H , the Henry's law
 9 constant, the sea-air OCS flux also depends on temperature, and was implemented in NEMO-
 10 PISCES following the expression established by Johnson et al. (1986):

$$11 \quad H = e^{\left(12722 - \frac{3496}{T}\right)} \quad (T \text{ in K}) \quad (12)$$

12 k_{water} is the piston velocity (in m.s^{-1}) for OCS. The coefficient is deduced from the Schmidt
 13 number of OCS and depends on surface wind speed, and is calculated with the relation of
 14 Wanninkhof (1992):

$$15 \quad k_{water} = [0.3u^2 + 2.5 * (0.5246 + 0.016256T + 0.00049946T^2)] * \sqrt{\frac{660}{S_{OCS}}} \quad (T \text{ in } ^\circ\text{C}) \quad (13)$$

16 Where u is the wind speed (in m.s^{-1}).

17 Note that Kettle et al. (2002) used similar parameterizations for the sea-surface exchange
 18 coefficient and the same relation from Wanninkhof et al. (1992) to model the global OCS flux
 19 at sea surface than the ones presented in this work.

20 The Schmidt number for OCS, S_{OCS} , dimensionless, was implemented in NEMO-PISCES
 21 following the suggestion by Ulshöfer (1995) to deduce it from kinetic viscosity (ν) and
 22 diffusion coefficient (D) (both in $\text{m}^2.\text{s}^{-1}$), respectively derived from:

$$23 \quad S_{OCS} = \frac{\nu}{D} \quad (14)$$

24 with:

$$25 \quad \nu = (1.792747 - 5.126103E^{-2}T + 5.918645E^{-4}T^2) * 1E^{-6} \quad (T \text{ in } ^\circ\text{C}) \quad (15)$$

$$26 \quad D = \left(10^{\left(\frac{-1010}{T}\right) - 1.3246}\right) * 1E^{-4} \quad (T \text{ in K}) \quad (16)$$

1 **2.3 An independent appraisal of photo-production rates**

2 Independently from NEMO-PISCES, the photochemical model of Fichot and Miller (2010)
3 was used to calculate monthly climatologies of depth-integrated photo-production rates of
4 OCS in the global ocean. Briefly, the photochemical model used three components to
5 calculate depth-resolved photochemical rates in the global ocean: 1) a radiative transfer model
6 for the determination of cloud-corrected UV-visible (290-490 nm) downward scalar
7 irradiance, 2) the SeaUV algorithm (Fichot et al., 2008), used to calculate the spectral diffuse
8 attenuation coefficient of UV and CDOM absorption coefficient (290-490 nm) from satellite
9 ocean color data, and 3) published AQY for the photochemical process of interest. To
10 describe the observed variability in AQY, both mean values from Weiss et al. (1995a) (open
11 ocean) and that of Zepp et al. (1994) (coastal ocean) were used in this study. Small
12 modifications to the original photochemical model were also made, including the use of
13 MODIS *Aqua* ocean color data (instead of SeaWiFS), and the use of a 2 nm spectral
14 resolution (instead of 5 nm). The photoproduction rates are later compared to the NEMO-
15 PISCES simulated rates and to other seawater measurements (e.g. Cutter et al., 2004).

16

17 **3 Results**

18 The absorption coefficient of CDOM at 350 nm (a_{350}) increased monotonically with
19 chlorophyll concentration for low chlorophyll contents. The different a_{350} -chlorophyll
20 relations used in this paper led to large differences in a_{350} estimates, especially at high
21 chlorophyll levels in seawater (Fig. 3). Estimates of a_{350} obtained with the relation based on
22 MODIS *aqua* ocean color, that we proposed (Eq.(6)), provided values two to three times
23 larger than a_{350} values obtained with the relation from Preiswerk et al. (2000). Since both
24 photo- and dark-production are modeled as linear functions of a_{350} ,
25 underestimating/overestimating chlorophyll concentrations directly lead to
26 underestimated/overestimated OCS production. Therefore, the evaluation of chlorophyll
27 concentration is of capital importance in the present work.

28 **3.1 Evaluation of chlorophyll concentration at the global scale**

29 Modeled annual mean surface chlorophyll concentrations from NEMO-PISCES compared
30 relatively well with SeaWiFS chlorophyll observations (Fig.4). The model correctly
31 represented main spatial patterns with for instance high latitudes showing higher annual mean
32 chlorophyll concentrations and a stronger seasonal cycle. Observed mid- and high-latitude

1 chlorophyll levels showed values three to four times larger than chlorophyll levels in tropical
2 regions, which was also well captured with NEMO-PISCES. However, the model generally
3 underestimated the chlorophyll concentration in the most oligotrophic subtropical zones of the
4 global ocean.

5 **3.2 Evaluation of the depth-distribution of a_{350} and OCS concentrations**

6 In order to provide an evaluation of modeled vertical distributions of OCS concentrations, in
7 this subsection we present vertical monthly mean profiles of a_{350} and OCS concentration from
8 1D simulation runs with NEMO-PISCES. Wherever possible, we compared these simulated
9 profiles with relevant in situ measurements. A majority of them were taken in the site of
10 BATS (31°N, 64°W). In situ measurements for OCS concentrations remain scarce at this
11 point. Evaluations of the contribution of each individual OCS formation and destruction
12 processes are even scarcer. Therefore, the cruise measurements around the BATS site from
13 Cutter et al. (2004) are often used as a reference.

14 **3.2.1 Vertical profiles for a_{350}**

15 Our MODIS-*Aqua* based extrapolation (Eq. (6)) resulted in the highest values of simulated
16 a_{350} (up to 0.15 m^{-1} , both in January and in August), while the parameterization from
17 Preiswerk et al.(2000) resulted in a_{350} values that were about half as much (Fig. 5), consistent
18 with the difference in the respective a_{350} -chlorophyll formulations (Fig. 3). Values for a_{350}
19 deduced from Morel and Gentili (2009) (Eq. (2)) gave an intermediary result. The pronounced
20 August maximum around 80 m depth (Fig. 5, B) reflected a chlorophyll content maximum at
21 this depth (a_{350} is monotonically increasing for low levels of chlorophyll). On the contrary,
22 low a_{350} values near the surface translated to a local minimum in the chlorophyll content. Note
23 also the abrupt decrease of chlorophyll concentrations, and therefore the decreasing a_{350} , for
24 depths below 80 m in August. In January the mixed layer was 120m-thick in NEMO-PISCES
25 at the BATS site (Fig. 5, A). Chlorophyll content (thus a_{350}) remained high and constant over
26 the first 120 m of the ocean before an abrupt decrease in the pycnocline. For both January and
27 August, chlorophyll concentrations and a_{350} values became negligible below 200m, with the
28 exception of a_{350} calculated with the relation proposed in this work.

29

30 **3.2.2 Vertical OCS concentration profiles**

1 Differences in a_{350} estimations using the relations in Eq. (2) to Eq. (6) led to 3-fold difference
2 between the most extreme near-surface OCS maximum concentrations simulated by NEMO-
3 PISCES (from 100 to 300 pmol L^{-1} in August and from 30 to 85 pmol L^{-1} in January). In the
4 photic zone (the first 30 m below the surface, as implemented in NEMO-PISCES), August
5 subsurface OCS concentrations (Fig. 5, D) were clearly driven by the photo-production
6 (vertical profile of photo-production not shown here). Where the influence of UV-light
7 irradiance is smaller or negligible (below 30 m in August or in the entire water column in
8 January), OCS concentration profiles are driven by the predominant dark-production (vertical
9 profile of the dark-production contribution not shown here). Therefore, in these layers, OCS
10 concentrations mostly followed the chlorophyll content profiles. Thus, OCS concentration
11 profiles simulated with NEMO-PISCES in January showed a drop below the mixed layer
12 (below 120m), and became negligible below 200m. In August, the highest concentrations
13 were found at the surface. A second peak of OCS levels was found around 80 m depth, where
14 chlorophyll content peaks. Deeper, the OCS concentrations decreased, down to negligible
15 values below 200m.

16 OCS concentrations simulated with NEMO-PISCES showed very large values in the few first
17 meters under the surface, averaging 70, 90 or even 270 pmol L^{-1} in August at BATS site,
18 depending on the a_{350} -chlorophyll relation used. Some OCS levels measured with buoys
19 during a field campaign in August 1999 at BATS peaked at 150 pmol L^{-1} in the first 3 meters
20 (Cutter et al. 2004), showing a potential to reach such high values. When using the a_{350}
21 formulas derived from the studies of Morel and Gentili (2009) or Preiswerk (2000), the
22 simulated vertical profiles of OCS concentrations in the Sargasso Sea in August (Fig. 5D) fall
23 into the range of measured OCS concentrations reported by Cutter et al. (2004). This is
24 however not the case when using the a_{350} based on MODIS-aqua data which lead to the
25 highest simulated OCS concentrations (270 pmol L^{-1} at the sea surface) and seem to
26 overestimate the natural variability of the OCS concentrations, as measured in these waters.

27 The lower OCS concentrations in deeper layers reflected the quick removal of OCS by
28 hydrolysis in the model (vertical profile of the hydrolysis contribution not shown here). This
29 behavior fit well with the estimated short lifetime of the OCS molecule in marine waters,
30 ranging between 4 and 13.4 hours, according to the models of Elliot et al. (1989) and
31 Radford-Knoery and Cutter (1993), respectively.

32

1 3.3 Spatial and seasonal variability of OCS production and removal processes

2 3.3.1 Surface a_{350} patterns

3 Absorption coefficients of CDOM at 350 nm (a_{350}) simulated using NEMO-PISCES were
4 evaluated for the different formulations of a_{350} against the annual climatology of a_{350} derived
5 from MODIS *Aqua* ocean color as in Fichot and Miller (2010). The MODIS *Aqua*-derived
6 a_{350} (Fig. 6, panel A) showed minimal values in the subtropical gyres, and maximum values in
7 coastal regions and at high latitudes (higher than 45°N and 45°S). Note that the MODIS *Aqua*
8 derived values should not be considered as direct observations but only as an independent
9 estimate relying on a generic relation (i.e., a statistical model).

10 Regions where a_{350} was not accurately modeled also suffered from biases in simulated
11 chlorophyll values. Therefore the highest a_{350} values observed near the coasts were not
12 represented in NEMO-PISCES due to its limited spatial resolution. Additionally, the
13 simulated chlorophyll maps (thus those of a_{350} as well) showed a higher contrast between low
14 and high latitudes than the SeaWiFS derived observations (Fig. 4). In tropical regions (30°S-
15 30°N), especially in the Atlantic Ocean, the Indian Ocean and in the Western Pacific Warm
16 Pool, chlorophyll levels simulated by NEMO-PISCES were underestimated by a factor of two
17 compared to the SeaWiFS chlorophyll observations (Fig. 4). As these are regions of warm
18 ocean waters favorable to OCS dark-production, the consequence might be an
19 underestimation of OCS production in these regions. In regions showing low chlorophyll
20 concentrations, this underestimation translates to an approximately 30% underestimation of
21 the a_{350} value (depending on the a_{350} formulation used), which directly translates to an
22 equivalent underestimation of OCS dark- and photo-production, since both parameterization
23 linearly depend on a_{350} .

24 Finally, NEMO-PISCES-simulated chlorophyll levels at mid- and high-latitudes were similar
25 for northern and southern oceans, with average values around 0.5 mg m⁻³. However,
26 chlorophyll concentrations deduced from satellite observations showed average mid- and
27 high-latitude values around 0.2 mg m⁻³ in the Southern Hemisphere and 0.5 to 1 mg m⁻³ in the
28 Northern Hemisphere. Thus, the NEMO-PISCES model overestimated the chlorophyll
29 concentrations by a factor of 2 over most of the mid- and high-latitudes of the Southern
30 Hemisphere - especially in the Pacific Ocean and south of Australia (Fig. 4). Therefore, our
31 modeled OCS production in the Southern Hemisphere is likely overestimated.

32 The different a_{350} -chlorophyll relations used in the present work (Eq. (2), Eq. (3) and Eq.(6))
33 led to simulated values of a_{350} differing by as much as a factor of three. The CDOM

1 absorption coefficient values obtained with the formulations of Preiswerk et al. (2000) and
2 Morel and Gentili (2009) were similar to the MODIS-derived estimates for low- and mid-
3 latitudes (below 60°S and 60°N), but largely underestimated at high latitudes in the Northern
4 Hemisphere, with values two to three times smaller than the MODIS-derived estimates (Fig.
5 6). Conversely, the formulation presented in this work (Eq. (6)) correctly reproduced the
6 observed levels of a_{350} in the northern high latitudes, but clearly overestimated the values for
7 CDOM absorption coefficient at low latitudes and in the Southern Hemisphere: simulated a_{350}
8 values in some subtropical oligotrophic regions reached values three to four times higher than
9 the MODIS derived values.

10 **3.3.2 Photo-production rates**

11 In the present study, the a_{350} -dependent NEMO-PISCES model and the AQY dependent
12 photochemical model from Fichot and Miller (2010) were used to provide two independent
13 estimates of OCS photo-production rates. Sensitivity tests were performed on the annual
14 global OCS photo-production over the entire water column (from the sea surface to the ocean
15 floor). Both models were run with different formulations of a_{350} (NEMO-PISCES model) or
16 using different AQY (Fichot and Miller photochemical model) from the literature.

17 The AQY estimates used were collected in open ocean environments (Weiss et al., 1995a) and
18 coastal environments (Zepp et al., 1994), respectively. Large uncertainties around AQY
19 estimations depending on the measurement location led to large differences in the estimates of
20 global OCS photo-production. Global OCS photo-production modeled with Fichot and
21 Miller's model (2010) thus ranged from 876 to 5,500 GgS yr⁻¹ (Table 1). Extremely high
22 AQY values have been measured on the continental shelf (Cutter et al., 2004), but were not
23 considered appropriate to represent the global average ocean. Using this last value would have
24 led to 37,700 GgS yr⁻¹ of OCS global photoproduction, far above observed photo-production
25 levels and other model estimates.

26 Both the photochemical model from Fichot and Miller (2010) and the NEMO-PISCES model
27 led to similar spatial distributions of OCS photo-production (Fig. 7). Indeed, subtropical
28 regions are the major contributors in terms of yearly total photo-production of OCS, because
29 the photo-production rates were roughly constant through the entire year, whichever model
30 was used. However, the highest monthly photo-production rates were found in mid-latitude
31 regions (40-60°N and 40-60°S) during the period of maximum irradiance, with rates twice as
32 large as the nearly constant rates obtained in tropical regions, as can be seen in the time-
33 latitude diagram in Fig. 8 (panel A). Depending on the value of the driving parameter for the 2

1 models used (AQY or a_{350} , respectively), large uncertainties existed over the total quantities
2 of OCS photo-produced. Global photo-production of OCS for the NEMO-PISCES model and
3 the photochemical model from Fichot and Miller (2010) are compared in Table 1. When using
4 the a_{350} -based model NEMO-PISCES, the range of the global OCS photo-production was
5 reduced but still large, with estimates between 1,390 and 4,540 GgS yr⁻¹, depending on which
6 formulation was chosen to calculate a_{350} . These values were in rather good agreement with the
7 range obtained with the AQY-based photochemical model from Fichot and Miller (2010).
8 The photochemical model from Fichot and Miller and NEMO-PISCES showed lower OCS
9 photo-production rates than in situ measurements, irrespective of the a_{350} formulation. For
10 instance, Cutter et al. (2004) estimated August photo-production rates up to 10 or 15 pmol L⁻¹
11 h⁻¹ in the Sargasso Sea, which is above the values of 4 to 9 pmol L⁻¹ h⁻¹ obtained by running
12 the NEMO-PISCES model at the same location (with implemented Eq. (3) and Eq. (6)
13 respectively) (Fig. 7).

14 **3.3.3 Dark-production rates**

15 Dark-production is a linear function of a_{350} (Eq. (8)). However, temperature is the main driver
16 of global OCS dark-production as simulated by NEMO-PISCES. The time-latitude
17 representation of dark-production rates (Fig. 8, panel B) showed that the maximum values
18 were located at low latitudes, in warm marine waters, despite the fact that these regions
19 correspond to the lowest a_{350} values (Fig. 6). The dark-production rates in these regions
20 remained relatively constant throughout the year. On the contrary, chlorophyll-rich waters at
21 higher latitudes, leading to higher a_{350} values (Fig. 6) corresponded to colder marine waters
22 and thus limited dark-production rates (due to the temperature dependency in Eq. (8)).

23 Measurements from Von Hobe et al. (2001) at the BATS site showed dark-production rates of
24 1 to 1.5 pmol L⁻¹ h⁻¹. NEMO-PISCES results showed a very good agreement with this data,
25 with rates of 0.8 pmol L⁻¹ h⁻¹ in August at BATS (not shown). In the study of Cutter et al.
26 (2004), calculated dark-production rates reached 4 pmol L⁻¹ h⁻¹ in August, significantly above
27 the simulated range by NEMO-PISCES. Von Hobe et al. (2001) estimated that dark-
28 production produces around 50% of OCS at these low latitudes. In the NEMO-PISCES
29 model, dark-production only represented 34% of the OCS produced at low latitudes, and 66%
30 of OCS is photo-produced.

31 **3.3.4 Hydrolysis rates**

32 Figure 2 presents the hydrolysis reaction constant as a function of temperature for a given pH,
33 as given by the Kamyshny et al. (2003) and Elliott et al. (1989) formulations. Both
34 formulations relate the OCS hydrolysis to the OCS concentration and to the seawater pH (Eq.

1 (10a) and Eq. (10b)). At a given pH, the difference between the two formulations was leading
2 to a 50% difference in the hydrolysis constant for seawater temperatures above 12°C (Fig. 2).
3 A comparison between time-latitude maps of the hydrolysis rate (Fig. 8, panel C) and the
4 OCS concentration (in Fig A1) suggests that OCS hydrolysis rates in NEMO-PISCES are
5 largely driven by OCS concentrations. These spatio-temporal variation patterns only slightly
6 differ around the equator, where marine waters are somewhat less alkaline, which leads to a
7 limitation of the OCS hydrolysis rate through pH influence. Simulations run with two
8 different hydrolysis parameterizations (based on Eq. (10a) or Eq. (10b)) provide global OCS
9 emissions diverging by a factor of 2.5 (see Fig. 10).

10 **3.3.5 Evaluation of surface concentration patterns**

11 Maps of annual mean surface OCS concentration patterns at sea surface simulated with
12 NEMO-PISCES are presented on Fig. 9 (right column). NEMO-PISCES simulations
13 produced maximum annual mean OCS levels in equatorial and sub-tropical regions, where
14 dark-production was maximal and photo-production was constantly active. In low latitude
15 marine waters, OCS concentrations remained nearly constant throughout the year (Fig A1 and
16 Fig. 9). However, the model showed a strong seasonal variability of OCS concentrations for
17 mid- and high latitudes, with roughly a factor 10 difference between maximal and minimal
18 OCS concentration levels reached throughout the year. These spatial distributions and the
19 intra-annual variation amplitudes were relatively independent of the formulation used in
20 NEMO-PISCES to calculate a_{350} .

21 Modeled OCS concentrations were evaluated against observational data available in the
22 literature. OCS concentrations measured near European shores and estuarine regions over the
23 year, showed large spatial and temporal variability (Uher, 2006). The few measured OCS
24 concentrations in estuarine regions were close to 250 pmol L⁻¹ in winter and 430 pmol L⁻¹ in
25 summer, while smaller values were measured near shores, from 40 pmol L⁻¹ in winter to 100
26 pmol L⁻¹ in summer. Von Hobe et al. (2003) also measured summer OCS surface maximum
27 levels of 120 pmol L⁻¹, in an upwelling region near the Portuguese coast. When using the
28 MODIS-*Aqua*-based a_{350} formulation (Eq. (6)) which gives the best representation of a_{350} in
29 the region (Fig.6), simulated OCS concentrations near shores only reached values from 30
30 pmol L⁻¹ in winter to 100 pmol L⁻¹ in summer (Fig. 9). NEMO-PISCES matches correctly the
31 seasonal amplitude of OCS concentrations measured in these areas and represents quite
32 accurately the absolute values measured near the shores. However, as expected, the lack of
33 resolution of the model translates into an under-estimation of the estuarine concentrations.

1 As shown in the comparison done in the study of von Hobe et al. (2003), the reproduction of
2 the OCS depth profiles by their models was generally less accurate than that of surface data
3 because the models were tuned to fit the surface concentrations. In our study, the model was
4 not tuned to fit surface or depth concentrations. As NEMO-PISCES provides gridded monthly
5 mean concentrations of OCS on the entire water column, monthly mean concentrations of
6 OCS data series should, ideally, be used to evaluate the global simulations.

7 Unfortunately, a global database of sea surface OCS measurements and a procedure to
8 calculate sea surface OCS as a function of latitude, longitude, and month are not available in
9 the literature as, for example, for DMS (e.g. Kettle et al., 1999; Lana et al., 2011). The
10 assemblage of a global OCS database was not achievable in the framework of this project.
11 The evaluation of the modeled oceanic OCS concentrations that had been carried out is not
12 fully satisfactory because we implicitly accepted to compare modeled monthly mean
13 concentrations and discrete measurements.

14 With these caveats in mind, 150 OCS measurements classified according to location, date and
15 depth were gathered from the literature (Weiss et al., 1995a ; Ulshofer et al., 1996 ; Cutter et
16 al., 2004 ; Von Hobe et al., 2001 and 2003) and compared with the outputs from the model
17 run with its “standard” parameterization, as described in the discussion section. The results
18 are displayed in Fig. A2 and show that the outputs of the model generally overestimate the
19 measured concentrations by a factor of two to four at the sea surface (first 10m, A), especially
20 at sites where low concentrations were measured. In seawaters with high OCS concentration
21 measurements (higher than 100 pmol L⁻¹), the corresponding simulated concentrations were
22 generally underestimated, up to a factor of two. A better agreement between modeled and
23 observed concentrations is found with the subsurface data (below 10m, B).

24 This model-data comparison suggests that simulated OCS concentrations might be
25 overestimated in a significant way in surface waters, which might lead to an overestimation of
26 the simulated OCS outgassing fluxes (up to factors of two to four). However, the limited
27 spatial (many measurements were done around 40°N) and temporal (many measurements in
28 July and August) distribution of the measurements severely reduced the possibility for an
29 exhaustive model validation and for the identification of concentration biases in the model.
30 Furthermore, a large range of concentrations were measured even for sites close in latitude
31 and/or for measurements realized around the same period of the year. Finally, this over-
32 estimation might also compensate for the under-estimation in the OCS production in shallow
33 water, since the model is lacking an exhaustive representation of the estuarines regions.

1 The formulation used to calculate a_{350} values did not affect the global spatial distribution of
2 OCS concentrations, but it largely influenced the absolute value of the simulated OCS
3 concentrations. For instance, maximal OCS concentrations in tropical sub-surface waters were
4 estimated close to 300 pmol L^{-1} with the MODIS-*Aqua*-based a_{350} formulation (Eq. (6)), while
5 Morel and Gentili (2009) (Preiswerk et al., 2000)-based estimates only reached one half (one
6 third, respectively) of these modeled maximal concentrations (Fig. 9). Note that the
7 formulation of Morel and Gentili (2009) led to results that were in better agreement with the
8 campaign measurements described in section 3.2.2 (Cutter et al., 2004; von Hobe et al., 2001).

9

10 **4 Discussion**

11 The limited number of studies which have attempted to quantify OCS production and removal
12 processes individually have yielded widely differing results. Several parameterizations for
13 each process have been proposed and each parameterization remains poorly constrained. In
14 this section we present our “best guess” formulations for the individual OCS-related processes
15 in the NEMO-PISCES model.

16 Measurement campaigns used to determine dark-production functions are particularly scarce.
17 The dark-production parameterization that we used is related to the CDOM absorption
18 coefficient at 350 nm, as a parameterization of the link with organic matter content and
19 biological activity in marine environments. However, there is no rationale for dark-production
20 to be dependent of colored organic matter content (CDOM, chlorophyll) since this process
21 occurs at times when no light is available.

22 In a rare example of observation-based dark-production parameterization effort, von Hobe et
23 al. (2003) used an experimental setup that allows them to equate the OCS dark-production
24 rate to the hydrolysis rate, and thus expressed the first as a function of a measurement of the
25 latter. In their estimate of the hydrolysis rate, von Hobe et al. (2003) use the Elliott et al.
26 (1989) formulation for the OCS hydrolysis constant. Thus, our use of the von Hobe et al.
27 (2003) dark-production parameterization is consistent with the choice of the Elliott et al.
28 (1989) parameterization for OCS hydrolysis.

29 As previously described, simulated a_{350} values can be far from the observed values in warm
30 water regions depending on the a_{350} formulation used (Fig. 6). This potentially leads to the
31 largest errors in the dark-production rate estimates. In this context, we have found the Morel
32 and Gentili (2009) a_{350} parameterization to perform best when evaluated against a_{350} values

1 derived from MODIS-*Aqua* data at low latitudes, as well as at high latitudes in the Southern
2 Hemisphere (section 3.3.1). This formulation may, however, lead to an underestimation of
3 a_{350} at high latitudes in Northern Hemisphere.

4 We have chosen the Uher et al. (1997) formulation for photoproduction associated with the
5 Morel and Gentili parameterization for a_{350} (Eq. (2)) and the Elliott formulation for the
6 hydrolysis constant as the standard parameterizations for OCS processes in NEMO-PISCES,
7 based on the arguments above. Time-latitude diagrams for photo- and dark-production,
8 hydrolysis and surface OCS fluxes using these parameterizations are represented in Fig. 8.
9 The time-latitude diagram representing the surface layer OCS concentration with the same
10 settings is shown in Fig A1.

11 The standard run of NEMO-PISCES suggests most OCS is produced photochemically. Even
12 at low latitudes, where warm water regions favor dark-production of OCS, photo-production
13 represents 66% of OCS production pathway (Fig. 8). In this simulation, low latitudes are the
14 only regions where dark-production rates compensate for hydrolysis removal of OCS. The
15 highest annual mean OCS concentrations modeled using best guess parameterizations range
16 between 100 and 200 pmol L^{-1} and are encountered around the equator, especially in Central
17 and Eastern Pacific Ocean. At mid and high latitudes, simulated annual mean OCS
18 concentrations are included between 10 and 60 pmol L^{-1} . These regions show higher seasonal
19 amplitude in OCS concentrations, especially around 60°N and 40°S, where periods of
20 irradiance maxima (resp. minima) lead to simulated OCS concentrations of 150 pmol L^{-1}
21 (resp. 10 pmol L^{-1}). In these regions, simulated concentrations are largely consistent with in
22 situ measurements from Cutter et al. (2004) and Von Hobe et al. (2003).

23 Surface OCS concentrations simulated by NEMO-PISCES are the main driver of the model's
24 sea-air OCS fluxes (Fig. 8, panel D and Fig A1). The regions with the highest sea surface
25 OCS concentrations (tropics and mid-latitudes during maximal irradiance seasons) are the
26 regions emitting the largest quantities of OCS. Multiple measurement campaigns (Rasmussen,
27 Khalil and Hoyt, 1982; Ferek and Andreae, 1983; Uher, 2006) have shown that coastal
28 environments can have OCS concentrations 5 to 10 times higher than those measured at the
29 surface of open ocean waters in oligotrophic regions. As shown in Fig.6, MODIS-derived a_{350}
30 reach maximal values along shores but the NEMO-PISCES model does not represent these
31 localized maxima due to the poor model resolution in these regions. These narrow areas have

1 an important potential in OCS production and show under-estimated OCS concentrations in
2 NEMO-PISCES.

3 Air-sea exchange of OCS is also enhanced by warm surface waters and strong winds (Eq.
4 (11)). Both variables have a noticeable impact on the simulated OCS surface fluxes,
5 especially at low latitudes. In fact, NEMO-PISCES simulations show the highest OCS
6 emissions around the equator even if some mid- and high-latitude oceanic regions show
7 higher OCS sea surface concentrations for some periods of the year: OCS outgassing rates in
8 July along the Equator are twice as important as outgassing taking place in Northern mid-
9 latitudes in the same period (Fig. 8, panel D), despite the mid-latitudes showing surface OCS
10 concentrations 60% higher than those simulated around the Equator.

11 We have investigated the sensitivity of the sea-air fluxes to the parameterizations of OCS
12 production and removal processes. Global and regional annual sea-air OCS fluxes obtained in
13 these tests are summarized in Fig. 10. Simulated fluxes by Kettle et al. (2002) are also
14 represented on the figure 10 (black line) for comparison. While the different parameterization
15 choices lead to a large spread in the simulated OCS fluxes towards the atmosphere, NEMO-
16 PISCES consistently produces higher estimates of the global sea-air OCS fluxes than the ones
17 previously estimated by Kettle et al. (2002). Total emitted OCS simulated using the “best
18 guess” parameterization of NEMO-PISCES reaches 813 GgS yr^{-1} , far above the modeled
19 direct source of 40 GgS yr^{-1} from Kettle et al. (2002) and consistent with the revised global
20 oceanic flux based on atmospheric measurements and a model for leaf uptake, proposed by
21 Berry et al. (736 GgS yr^{-1}). Extrapolations of measurements carried out in the Mediterranean
22 sea and the Indian ocean by Mihalopoulos et al. (1992) led to an independent estimate of 213
23 GgS yr^{-1} , markedly lower than the mean annual global flux simulated with NEMO-PISCES.
24 Kettle et al. (2002) described the global direct exchange of OCS between the ocean and the
25 atmosphere as highly uncertain, and pointed out the fact that in some of their simulations,
26 some regions of the ocean behaved like sinks of atmospheric OCS at certain periods of the
27 year. Some regions at extreme high latitudes also act like a sink of atmospheric OCS in
28 NEMO-PISCES for certain periods of the year (Fig. 8, panel D).

29- The different parameterizations available for the different processes presented in this paper
30 lead to different global flux estimates, ranging from 573 GgS yr^{-1} (when using the CDOM
31 absorption coefficient values obtained with the formulations of Preiswerk et al. (2000) and the
32 higher values of the Elliot-based hydrolysis constant) to 3997 GgS yr^{-1} (when using the

1 MODIS-derived a_{350} and the lower values of the Kamyshny-based hydrolysis constant). Our
2 “best-guess” parameterization of NEMO-PISCES shows the best agreement with the in situ
3 evaluation of the individual processes, and stands in the lower part of the range of OCS direct
4 annual emissions by ocean at a global scale.

5- Changing the parameterization also changes the seasonal amplitude of the simulated OCS
6 flux by up to a factor five for Northern and Southern Hemisphere oceans but no significant
7 change is noticeable on the seasonal amplitude of OCS fluxes in the tropical region.

8 Recent efforts to constrain global OCS fluxes have led to a growing number of measurements
9 and consequent revisions of soil and vegetation uptake estimates. Multiple recent studies have
10 suggested that soil and vegetation uptakes were underestimated in the new assessments of the
11 global OCS cycle and have suggested a global sink for both of up to 1000 GgS yr⁻¹ (Berry et
12 al., 2013; Suntharalingam et al., 2008), much larger than the estimates of approximately 300
13 GgS yr⁻¹ by Kettle et al. (2002). Knowing that atmospheric OCS levels show no trend over the
14 last two decades (Montzka et al., 2007), the global cycle of OCS is expected to be balanced
15 on a global scale. In order to compensate re-estimated sinks based on a mechanistic
16 description of leaf OCS uptake (using SIB3 land surface model), Berry et al. (2013) have
17 suggested that the ocean provides the missing source. Using a simple inversion approach to
18 optimize the oceanic missing source, given known land natural and anthropogenic fluxes, the
19 authors evaluated that the ocean should emit 736 GgS yr⁻¹. Moreover, the best-fit optimization
20 used by the authors revealed that the missing source should be concentrated over the low
21 latitudes in order to best fit the atmospheric data recorded at NOAA stations.

22 Using our “best guess” parameterization for NEMO-PISCES leads to relatively constant
23 global OCS outgassing throughout the year, with a seasonal amplitude of only 10%. Tropical
24 regions (30°S-30°N) emit the major part of the OCS, and represent up to 45% of the total
25 emitted OCS towards the atmosphere. Tropical exchanges show almost no variation
26 throughout the year. Northern and southern oceanic regions at mid- and high latitudes (higher
27 than 30°N and 30°S, respectively) participate to 20% and 35%, respectively, of the OCS
28 global flux towards atmosphere each year (Fig A3).

29 Despite the consistency in terms of global OCS fluxes quantities and spatial distribution
30 between best guess parameterizations of NEMO-PISCES and indirect oceanic source estimate
31 from Berry et al. (2013), the simulated outgassing using NEMO-PISCES show a large
32 envelope when using the different possible parameterizations. Most of them lead to much

1 larger global flux estimates than previous studies, ranging between 573 and 3997 GgS yr⁻¹.
2 Higher estimates for OCS fluxes with NEMO-PISCES result from using hydrolysis constant
3 from Kamyshny et al. (2003) or a_{350} calculation proposed in this present work. Kamyshny-
4 based hydrolysis constant is not homogeneous with the choice of an Elliot-based hydrolysis
5 constant used to determinate OCS dark-production by von Hobe et al. (2001), as implemented
6 in NEMO-PISCES. Moreover, calculation of a_{350} proposed in this work was demonstrated to
7 lead to large over-estimations of the a_{350} values compared with the observational data. Both
8 parameterizations lead to very large estimates of OCS fluxes towards the atmosphere, which
9 are not likely since they would lead to highly unbalanced atmospheric OCS budget.

10

11 **5 Conclusion**

12 At a global scale, the ocean is supposed to be the largest direct and indirect source of OCS to
13 the atmosphere. Recent studies (Suntharalingam et al., 2008; Berry et al., 2013) pointed out
14 the need to re-evaluate the global OCS sinks, signaling a possible underestimation in previous
15 assessments. There is currently no trend in the atmospheric levels of OCS (Montzka et al.,
16 2007), thus increased sinks have to be compensated by a source, currently missing from the
17 global OCS budget. The recent inversion study of Berry et al. (2013) and previous
18 Atmospheric Chemistry Experiment ACE observational analysis of Barkley et al. (2008) have
19 suggested that a large part of this missing source should be ocean outgassing at low latitudes.
20 Previous studies of the OCS production and removal processes in the ocean have only led to
21 poor constraint of the potential global sea-air fluxes. Moreover, numerical simulations have
22 led to relatively small modeled global fluxes of OCS outgassed to the atmosphere. In this
23 study we have selected different parameterizations for the most important OCS production
24 and removal processes, which we then implemented in the 3D NEMO-PISCES ocean model.
25 Simulated fluxes with this model showed a potential for large global OCS fluxes, with our
26 best guess simulation reaching a net emission of OCS up to 800 GgS yr⁻¹, much larger than
27 previous estimated ranges. Moreover, the resulting spatial distribution of these fluxes
28 supports the assumed key role of tropical regions, where warm marine waters can produce
29 high levels of OCS with little organic matter. Our modeled ocean-atmosphere OCS fluxes
30 were concentrated in the equatorial and subtropical regions, which accounted for half of the
31 global OCS outgassing to the atmosphere. This result is in good agreement with the necessary
32 distribution of the missing oceanic source of OCS that would be consistent with the
33 atmospheric OCS concentration gradients (north south gradient for instance), measured at the

1 different stations of the NOAA network. The uncertainties around OCS fluxes, however, will
2 remain very large until a wide array of measurements focusing on the individual processes is
3 available, to accurately calibrate the relative importance of each marine OCS production and
4 removal process.

5

6 **Authors contribution**

7 S. Belviso and P. Peylin designed the experiments. T. Launois did the bibliography research
8 for process parameterizations and developed the NEMO-PISCES specific OCS module code
9 and performed the simulations with the help from L. Bopp. C. Fichot run tests with the
10 SeaUV model that he developed, allowing comparison of OCS photo-production rates with
11 the results obtained with NEMO-PISCES. T. Launois prepared the manuscript with
12 contributions from all co-authors.

13

14 **Acknowledgements**

15 The authors wish to thank Elliott Campbell who shared simulation results from Kettle et al.
16 (2002) and allowed the comparisons done in this work. We also thank Alina Gainusa-Bogdan
17 for improving the manuscript.

18 **References**

- 19 Aumont, O., and L. Bopp, Globalizing results from ocean in situ iron fertilization studies,
20 GLOBAL BIOGEOCHEM CY, 20, GB2017, doi:[10.1029/2005GB002591](https://doi.org/10.1029/2005GB002591), 2006
- 21 Barnes, I., Becker, K. H., Patroescu, I. The tropospheric oxidation of dimethyl sulfide: A new
22 source of carbonyl sulfide. GEOPHYS RES LETT., 21(22), 2389-2392, 1997
- 23 Bopp L., Aumont O., Belviso S., Blain S, Modelling the effect of iron fertilization on
24 dimethylsulphide emissions in the Southern Ocean. DEEP-SEA RES PT II, 55(5), 901-912,
25 2008
- 26 Barkley M. P., Palmer P. I., Boone C. D., Bernath P. F. and Suntharalingam P., Global
27 distributions of carbonyl sulfide in the upper troposphere and stratosphere. GEOPHYS RES
28 LETT, 35, L14810, doi:[10.1029/2008GL034270](https://doi.org/10.1029/2008GL034270), 2008
- 29 Berry J., Wolf A., Campbell J. E., Baker I., Blake N., Blake D., Zhu, Z., A coupled model of
30 the global cycles of carbonyl sulfide and CO₂: A possible new window on the carbon cycle. J
31 GEOPHYS RES-BIOGEO, 118(2), 842-852, 2013

- 1 Bricaud A., Babin M., Morel A., Claustre H., Variability in the chlorophyll-specific
2 absorption coefficients of natural phytoplankton: Analysis and parameterization. *J GEOPHYS*
3 *RES-OCEANS*, (1978–2012),100(C7), 13321-13332, 1995
- 4 Brühl C., Lelieveld J., Crutzen P. J., Tost H., The role of carbonyl sulphide as a source of
5 stratospheric sulphate aerosol and its impact on climate. *ATMOS CHEM PHYS*, 12(3), 1239-
6 1253, 2012
- 7 Campbell J. E., Carmichael G. R., Chai T., Mena-Carrasco M., Tang Y., Blake D. R., Stanier
8 C. O., Photosynthetic control of atmospheric carbonyl sulfide during the growing
9 season. *SCIENCE*, 322(5904), 1085-1088, 2008
- 10 Chin M., Davis D. D., A reanalysis of carbonyl sulfide as a source of stratospheric
11 background sulfur aerosol. *J GEOPHYS RES-OC ATMOS* (1984–2012), 100(D5), 8993-
12 9005, 1993
- 13 Cutter G. A., Cutter L. S., Filippino K. C., Sources and cycling of carbonyl sulfide in the
14 Sargasso Sea. *LIMNOL OCEANOGR*, 49(2), 555-565, 2004
- 15 Elliott S., Lu E., Rowland F. S., Rates and mechanisms for the hydrolysis of carbonyl sulfide
16 in natural waters. *ENVIRON SCI TECHNOL*, 23(4), 458-461, 1989
- 17 Ferek R. J., Andreae M. O., Photochemical production of carbonyl sulphide in marine surface
18 waters, *GLOBAL BIOGEOCHEM CY*, 6(2), 175–183, 1984
- 19 Fichot C. G., Miller W. L., An approach to quantify depth-resolved marine photochemical
20 fluxes using remote sensing: Application to carbon monoxide (CO)
21 photoproduction. *REMOTE SENS ENVIRON*, 114(7), 1363-1377, 2010
- 22 Fichot C. G., Sathyendranath S., Miller W. L., SeaUV and SeaUVC: Algorithms for the
23 retrieval of UV/Visible diffuse attenuation coefficients from ocean color. *REMOTE SENS*
24 *ENVIRON*, 112(4), 1584-1602, 2008
- 25 Flöck O. R., Andreae M. O., Dräger M., Environmentally relevant precursors of carbonyl
26 sulfide in aquatic systems. *MAR CHEM*, 59(1), 71-85, 1997
- 27 Johnson J. E., Harrison H., Carbonyl sulfide concentrations in the surface waters and above
28 the Pacific Ocean. *J GEOPHYS RES-OC ATMOS* (1984–2012), 91(D7), 7883-7888, 1986
- 29 Kamyshny A., Goifman A., Rizkov D., Lev O., Formation of carbonyl sulfide by the reaction
30 of carbon monoxide and inorganic polysulfides. *ENVIRON SCI TECHNOL*, 37(9), 1865-
31 1872, 2003
- 32 Kettle, A. J., et al. (1999), A global database of sea surface dimethylsulfide (DMS)
33 measurements and a procedure to predict sea surface DMS as a function of latitude, longitude,
34 and month, *Global Biogeochem. Cycles*, 13(2), 399–444, doi:
- 35 Kettle A. J., Kuhn U., Hobe M. V., Kesselmeier J., Liss P. S., Andreae M. O., Comparing
36 forward and inverse models to estimate the seasonal variation of hemisphere-integrated fluxes
37 of carbonyl sulfide. *ATMOS CHEM PHYS*, 2(5), 343-361, 2002
- 38 Kloster S., Feichter J., Maier-Reimer E., Six K. D., Stier P., Wetzell P., DMS cycle in the
39 marine ocean-atmosphere system? a global model study. *BIOGEOSCIENCES*, 3(1), 29-51,
40 2006

- 1 Lana, A., et al. (2011), An updated climatology of surface dimethylsulfide concentrations and
2 emission fluxes in the global ocean, *Global Biogeochem. Cycles*, 25, GB1004,
3 doi:[10.1029/2010GB003850](https://doi.org/10.1029/2010GB003850)
- 4 Large W. G., Yeager S. G., The global climatology of an interannually varying air–sea flux
5 data set, *CLIM DYNAM*, 33, 341–364, 2008
- 6 Madec G., NEMO ocean general circulation model reference manuel. Internal Report.
7 LODYC/IPSL, Paris, 2008
- 8 Mihalopoulos N., Nguyen B. C., Putaud J. P., Belviso S., The oceanic source of carbonyl
9 sulfide (COS). *ATMOS ENVIRON A-GEN*, 26(8), 1383-1394, 1992
- 10 Morel A., Optical modeling of the upper ocean in relation to its biogenous matter content
11 (case I waters). *J GEOPHYS RES-OCEANS* (1978–2012), 93(C9), 10749-10768, 1988
- 12 Morel A., Gentili B., A simple band ratio technique to quantify the colored dissolved and
13 detrital organic material from ocean color remotely sensed data. *REMOTE SENS*
14 *ENVIRON*, 113(5), 998-1011, 2009
- 15 Montzka S. A., Calvert P., Hall B. D., Elkins J. W., Conway T. J., Tans P. P., Sweeney, C.,
16 On the global distribution, seasonality, and budget of atmospheric carbonyl sulfide (COS) and
17 some similarities to CO₂. *J GEOPHYS RES-OC ATMOS* (1984–2012), 112(D9), 2007
- 18 Notholt J., Weisenstein D., Kuang Z., Rinsland C. P., Toon G. C., Rex M., Schrems O.,
19 Composition of the upper tropical troposphere and its influence on the stratospheric aerosol
20 formation. *EGS-AGU-EUG Joint Assembly* (Vol. 1, p. 4024), 2003
- 21 Para J., Coble P.G., Charrière B., Tedetti M., Fontana C., Sempéré R., Fluorescence and
22 absorption properties of chromophoric dissolved organic matter (CDOM) in coastal surface
23 waters of the northwestern Mediterranean Sea, influence of the Rhône River.
24 *BIOGEOSCIENCES*, 7, 4083-4103, 2010
- 25 Preiswerk D., Najjar R. G., A global, open-ocean model of carbonyl sulfide and its air-sea
26 flux. *GLOBAL BIOGEOCHEM CY*, 14(2), 585-598, 2000
- 27 Radford-Knoery J., Cutter G. A., Determination of carbonyl sulfide and hydrogen sulfide
28 species in natural waters using specialized collection procedures and gas chromatography
29 with flame photometric detection. *ANAL CHEM*, 65(8), 976-982, 1993
- 30 Rasmussen R. A., Khalil M. A. K., Hoyt S. D., The oceanic source of carbonyl sulfide
31 (OCS). *ATMOS ENVIRON* (1967), 16(6), 1591-1594, 1982
- 32 Suntharalingam P., Kettle A. J., Montzka S. M., Jacob D. J., Global 3-D model analysis of the
33 seasonal cycle of atmospheric carbonyl sulfide: Implications for terrestrial vegetation
34 uptake. *GEOPHYS RES LETT*, 35(19), 2008
- 35 Tedetti M., Sempéré R., Penetration of ultraviolet radiation in the marine environment. A
36 review. *PHOTOCHEM PHOTOBIOLOG*, 82(2), 389-397, 2006
- 37 Uher G., Distribution and air–sea exchange of reduced sulphur gases in European coastal
38 waters. *ESTUAR COAST SHELF S*, 70(3), 338-360, 2006

1 Uher G., Andreae M. O., Photochemical production of carbonyl sulfide in North Sea water: A
2 process study. *LIMNOL OCEANOGR*, 42(3), 432-442, 1997

3 Ulshöfer V. S., Uher G., Andreae M. O., Evidence for a winter sink of atmospheric carbonyl
4 sulfide in the northeast Atlantic Ocean. *GEOPHYS RES LETT*, 22(19), 2601-2604, 1995

5 Ulshöfer V. S., Flock O. R., Uher G., Andreae M. O., Photochemical production and air-sea
6 exchange of carbonyl sulfide in the eastern Mediterranean Sea. *MAR CHEM*, 53(1), 25-39,
7 1996

8 Von Hobe M., Cutter G. A., Kettle A. J., Andreae M. O., Dark production: A significant
9 source of oceanic COS. *J GEOPHYS RES-OCEANS* (1978–2012), 106(C12), 31217-31226,
10 2001

11 Von Hobe M., Najjar R. G., Kettle A. J., Andreae M. O., Photochemical and physical
12 modeling of carbonyl sulfide in the ocean. *J GEOPHYS RES-OCEANS* (1978–
13 2012), 108(C7), 2003

14 Wanninkhof R., Relationship between wind speed and gas exchange over the ocean. *J*
15 *GEOPHYS RES-OCEANS* (1978–2012), 97(C5), 7373-7382, 1992

16 Watts S. F., The mass budgets of carbonyl sulfide, dimethyl sulfide, carbon disulfide and
17 hydrogen sulfide. *ATMOS ENVIRON*, 34(5), 761-779, 2000

18 Weiss P. S., Johnson J. E., Gammon R. H., Bates T. S., Reevaluation of the open ocean source
19 of carbonyl sulfide to the atmosphere. *J GEOPHYS RES-OC ATMOS* (1984–
20 2012), 100(D11), 23083-23092, 1995a

21 Weiss P. S., Andrews S. S., Johnson J. E., Zafiriou O. C., Photoproduction of carbonyl sulfide
22 in South Pacific Ocean waters as a function of irradiation wavelength. *GEOPHYS RES*
23 *LETT*, 22(3), 215-218, 1995b

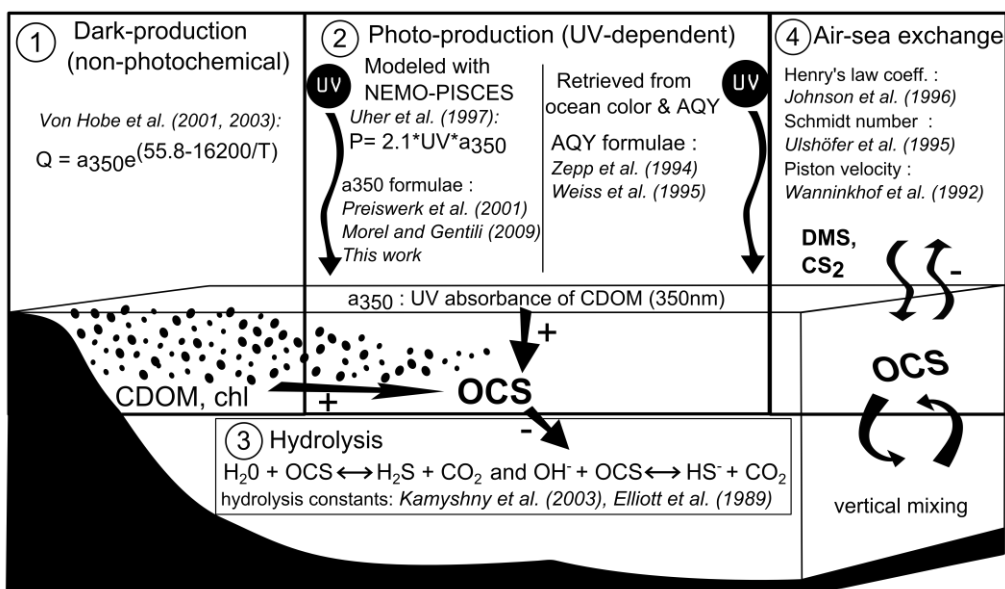
24 Wohlfahrt G., Brilli F., Hörtnagl L., Xu X., Bingemer H., Hansel A., Loreto F., Carbonyl
25 sulfide (COS) as a tracer for canopy photosynthesis, transpiration and stomatal conductance:
26 potential and limitations†. *PLANT CELL ENVIRON*, 35(4), 657-667, 2012

27 Xu X., Bingemer H. G., Georgii H. W., Schmidt U., Bartell, U., Measurements of carbonyl
28 sulfide (COS) in surface seawater and marine air, and estimates of the air-sea flux from
29 observations during two Atlantic cruises. *J GEOPHYS RES-OC ATMOS* (1984–
30 2012), 106(D4), 3491-3502, 2001

31 Zepp R. G., Andreae M. O., Factors affecting the photochemical production of carbonyl
32 sulfide in seawater. *GEOPHYS RES LETT*, 21(25), 2813-2816, 1994

33
34
35
36
37
38

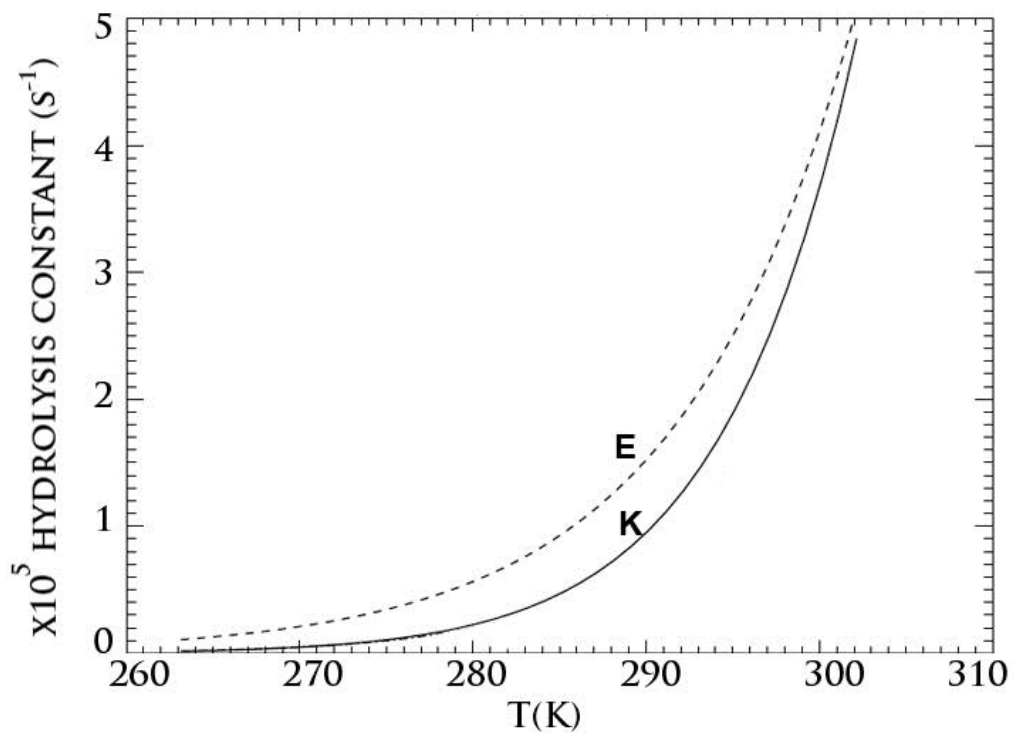
1
2
3
4
5
6
7
8
9



10

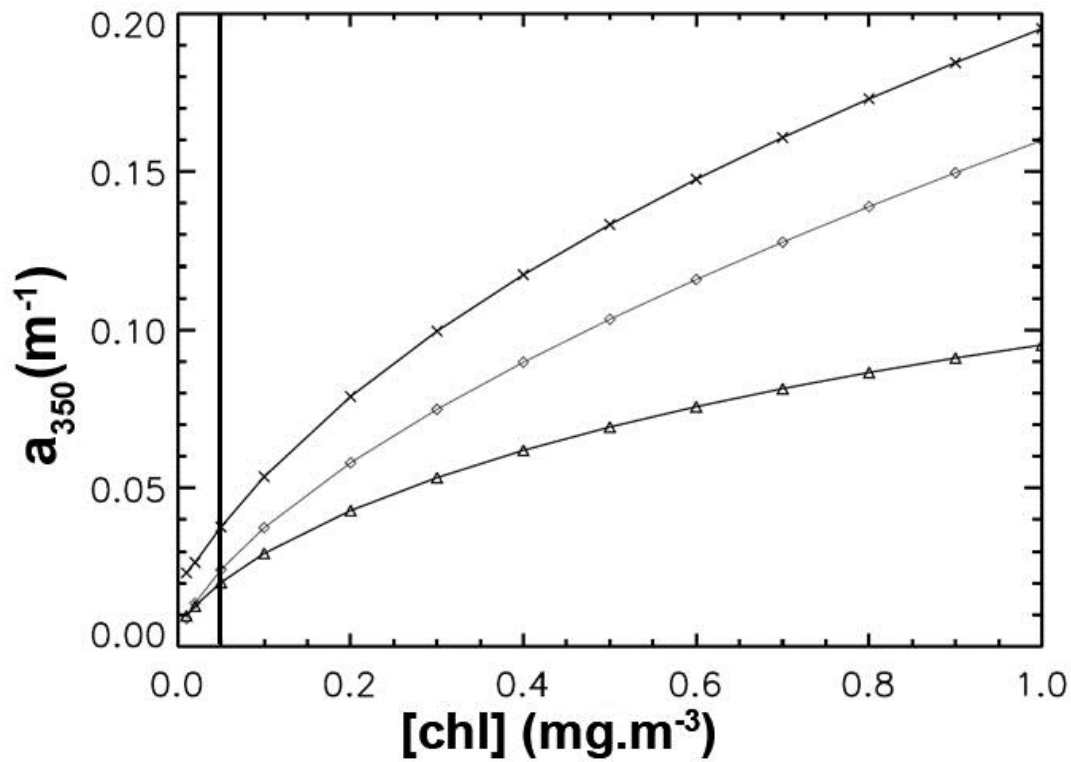
11 Figure 1: Main production and removal processes implemented in the NEMO-PISCES
 12 OGCM to simulate the marine OCS cycle: dark-production, photo-production and hydrolysis.
 13 Of central importance is the UV absorption coefficient at 350 nm of chromophoric dissolved
 14 organic matter (CDOM) which is derived from modeled Chl concentrations using three
 15 different relationships linking a_{350} to Chl. The simulated photo-production rates of OCS were
 16 evaluated independently using the model of Fichot and Miller (2010) and published apparent
 17 quantum yields (AQY). Aqueous OCS is removed by hydrolysis (two different formulations
 18 of the hydrolysis rate are used), lost or absorbed at the air-sea interface and mixed both
 19 vertically and horizontally. Studies relevant for sensitivity tests and model parameterization
 20 presented in this paper are displayed in *italic*. Oceans also emit DMS and CS₂ which are later

1 oxidized in OCS in the atmosphere. These indirect sources of OCS are not detailed in the
2 present study.



3
4 Figure 2: Temperature dependence of hydrolysis rates implemented in NEMO-PISCES. The
5 relationships are represented for pH = 8.2, and taken from Elliott et al. (1989) (E, dashed line)
6 or Kamyshny et al. (2003) (K, solid line). .

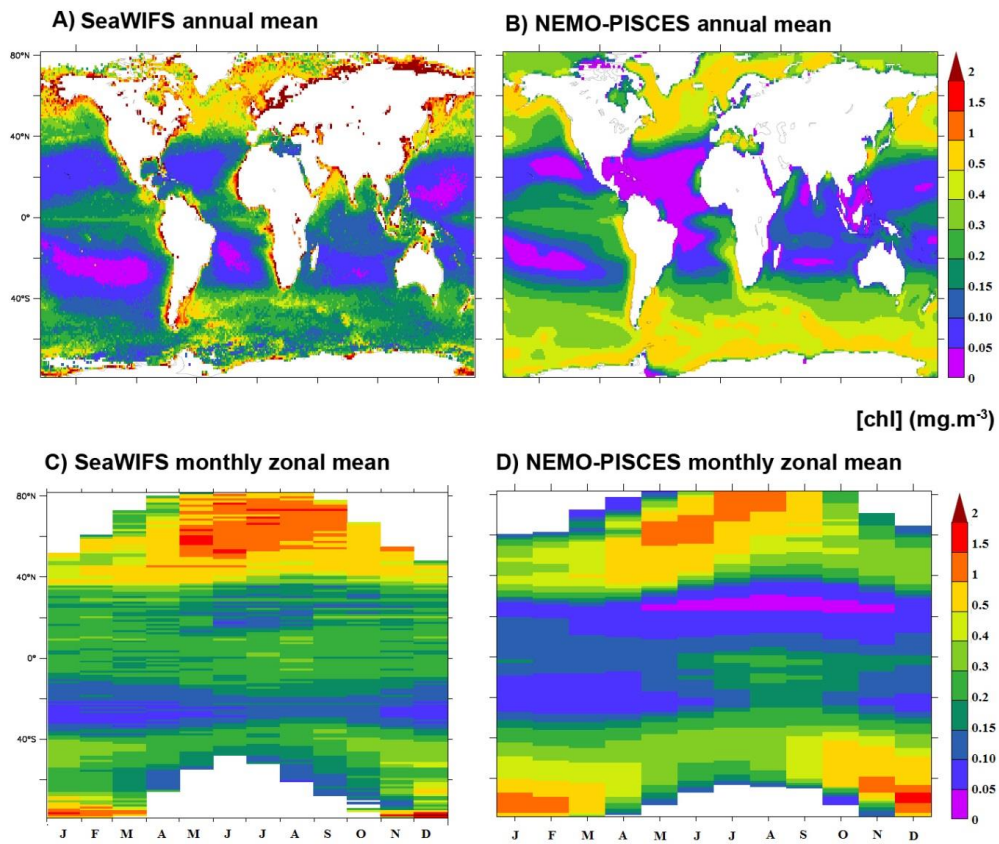
7
8
9
10
11
12
13



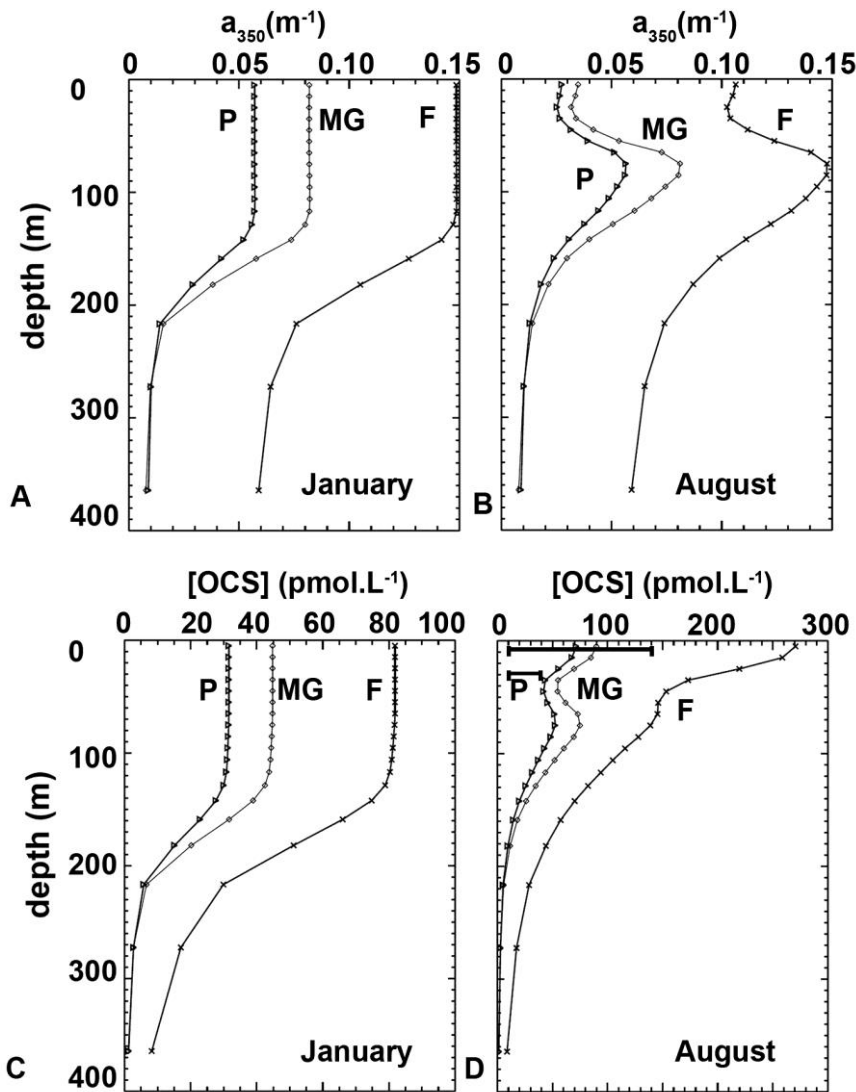
1
 2 Figure 3: Relationships implemented in the NEMO-PISCES model between UV absorption
 3 coefficients for CDOM at 350 nm and chlorophyll concentrations. The 3 respective
 4 relationships are from Morel and Gentili (2009) (diamonds), Preiswerk et al. (2000)
 5 (triangles) or issued from this study, based on MODIS-Aqua ocean color (crosses).
 6 Chlorophyll concentrations in NEMO-PISCES have a fixed minimal value of 0.05 mg.m⁻³
 7 (thick vertical line).

8

9

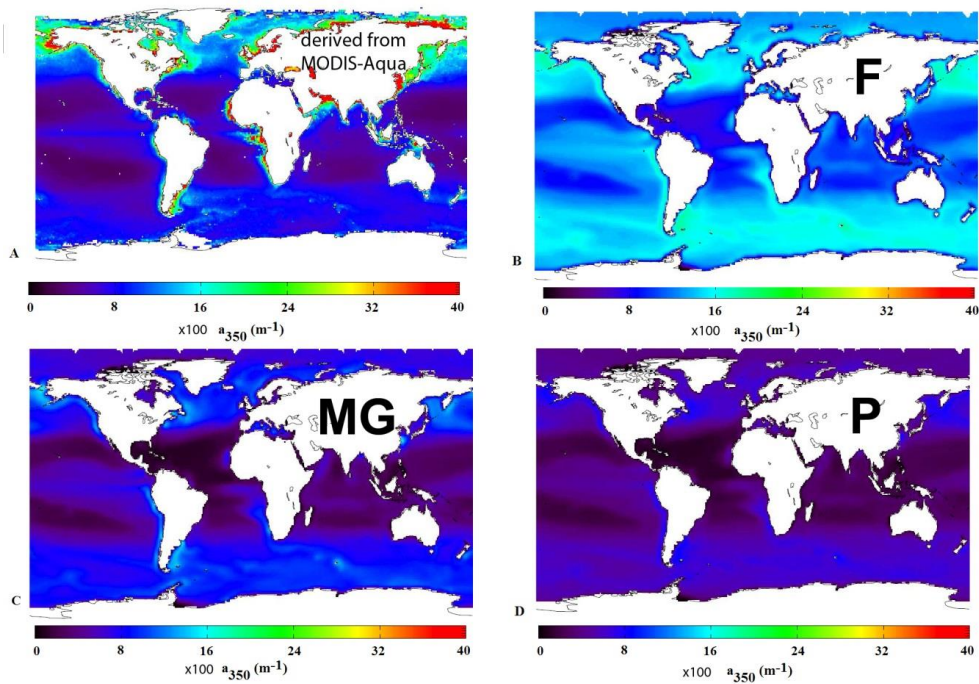


1
 2 Figure 4: Comparison of remotely sensed observations of chlorophyll (left panels) with
 3 simulations performed using the NEMO-PISCES model (right panels). Top panels (a, b)
 4 represent maps of annual mean chlorophyll concentration ($\text{mg}\cdot\text{m}^{-3}$). Bottom panels (c, d)
 5 represent latitude-time maps of chlorophyll.
 6



1
2 Figure 5: Monthly mean vertical profiles of a_{350} (top row) and OCS concentration (bottom
3 row) in January (left column) and August (right column) simulated by NEMO-PISCES in a 1-
4 D run at the Bermuda Atlantic Time Series (BATS) site. The thick lines on figure D cover the
5 range between minimal and maximal values as measured by Cutter et al. (2004). The different
6 a_{350} profile are calculated using the formulations of Morel and Gentili (2009) (MG,
7 diamonds), Preiswerk et al. (2000) (P, triangles) or based on MODIS-*aqua* data (F, black
8 line). Symbols used on OCS concentration profile on bottom row indicate which a_{350} -
9 chlorophyll relation was used in the simulation.

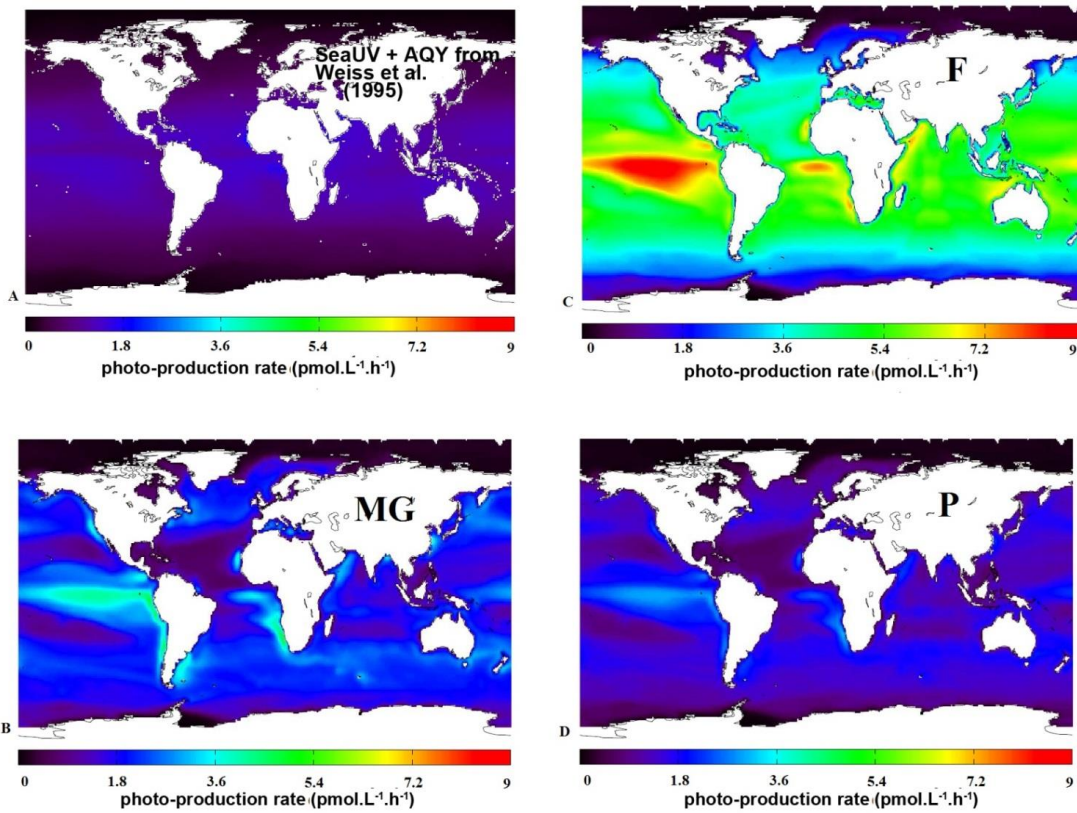
10



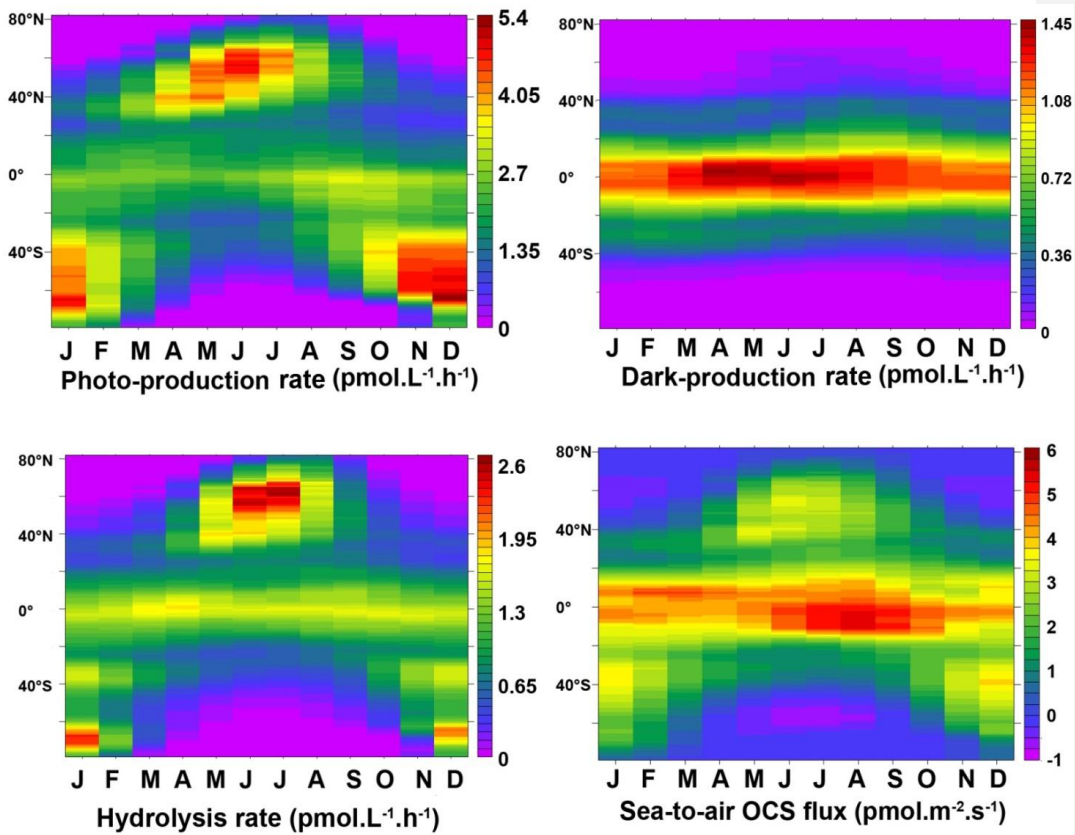
1

2 Figure 6: Comparison between annual mean surface absorption coefficient of CDOM at 350
 3 nm: (A) retrieved from MODIS-*Aqua* satellites data, using SeaUV model (Fichot et al., 2008)
 4 and a_{320}/K_{d320} ratio from Fichot and Miller (2010) and a_{350} maps simulated with the NEMO-
 5 PISCES model using the relation described in Morel and Gentili (2009) (MG, panel C),
 6 Preiswerk et al. (2000) (P, panel D) or proposed in this work (F, panel B).

7



1
 2 Figure 7: Annual mean photo-production rates integrated over the entire water column
 3 simulated with the photochemical model of Fichot and Miller (2010) and using the apparent
 4 quantum yield of Weiss et al (1995a) (panel A). Comparison with annual mean photo-
 5 production rates integrated over the entire water column simulated with the NEMO-PISCES
 6 model using a_{350} formulations from Morel and Gentili (2009) (panel C), Preiswerk et al.
 7 (2000) (panel D) or proposed in this study (panel B).
 8



1

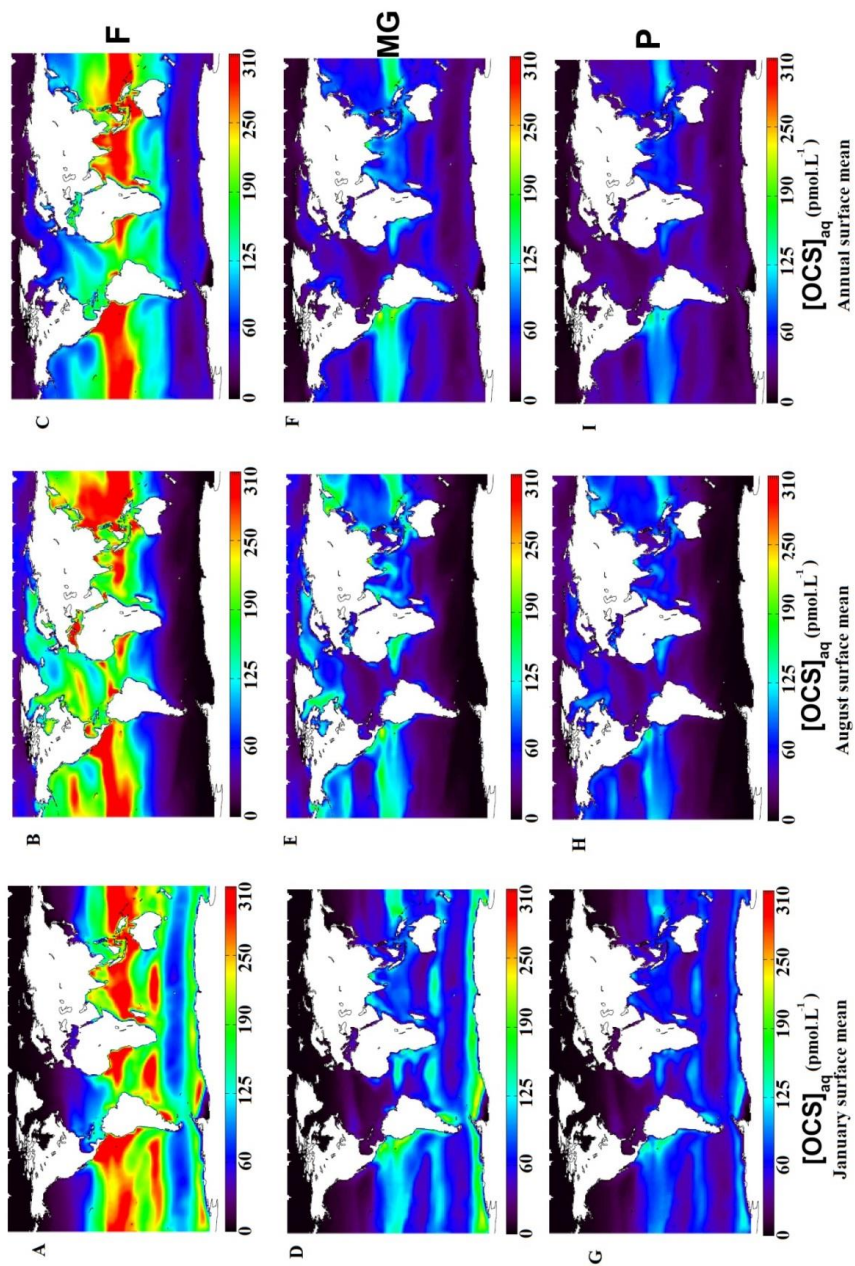
2 Figure 8: Latitude-time plots comparing relative importance of individual processes for OCS
 3 production (top row) and removal (bottom row) in NEMO-PISCES surface layer. Sea-air
 4 exchanges are displayed in bottom right panel are displayed with positive fluxes when OCS is
 5 outgassed towards the atmosphere. All runs were performed using Morel and Gentili (2009)
 6 formulation to calculate a_{350} and Elliott et al. (1989) formulation of hydrolysis constant.

7

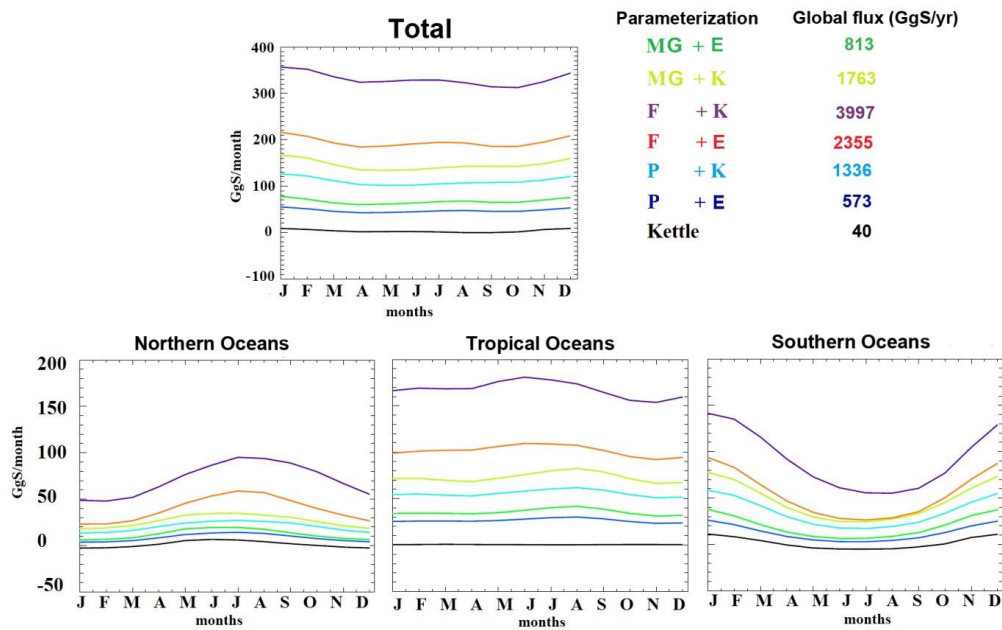
8

9

10



1
 2 Figure 9: Monthly mean surface OCS concentrations for January (left column), August
 3 (central column) and annual mean (right column) simulated with NEMO-PISCES. The three
 4 simulations differ in the relationship used to calculate a_{350} from chlorophyll: MODIS *Aqua*-
 5 derived, proposed in this study (F, upper row), from Preiswerk et al. (2000)(P, central row) or
 6 Morel and Gentili (2009)(MG, lower row).



1

2 Figure 10: Global and regional monthly mean sea-air fluxes for 6 different parameterizations
 3 of the NEMO-PISCES model. Kettle et al. 2002 (black line) is shown as a reference. Each
 4 colored line represents a set of parameters: first name refers to the equation used to calculate
 5 the UV absorption coefficient of CDOM at 350 nm and the second name refers to the
 6 hydrolysis constant formulation. Global fluxes on top row, Northern Oceans (30°N-90°N,
 7 bottom left), Tropical region (30°S-30°N, bottom center), Southern Oceans (30°S-90°S,
 8 bottom right). F: a_{350} relation assembled in this study; MG: a_{350} relation from Morel and
 9 Gentili (2009); P: a_{350} relation from Preiswerk et al. (2000); E: hydrolysis constant from
 10 Elliott et al. (1989); K: hydrolysis constant from Kamyshny et al. (2003)

11

12

13

14

15

16

17

18

1 Table 1: Annual global photo-production of OCS in the entire water column simulated with
 2 the NEMO-PISCES model (using the three different a_{350} formulations presented in this paper)
 3 or with the photochemical model derived from Fichot and Miller (2010) (FM in the
 4 table)(using two different apparent quantum yields estimates). F: a_{350} parameterization
 5 assembled in this work; MG: a_{350} parameterization presented in Morel and Gentili (2009); P:
 6 a_{350} parameterization presented in Preiswerk et al. (2000).

Parameterization used in the runs	Total photo-produced OCS in the entire water column (GgS yr⁻¹)
NEMO-PISCES + F	4540
NEMO-PISCES + MG	1910
NEMO-PISCES + P	1390
FM + AQY from Weiss et al. (1995a)	876
FM + AQY from Zepp et al. (1994)	5500

7
8
9
10
11
12
13
14
15
16
17
18
19
20
21
22
23
24
25
26

1 Table 2: Yearly global OCS flux emitted from ocean to the atmosphere (in GgS yr⁻¹)
 2 depending on the different parameterizations presented in previous work and in this work. F:
 3 a₃₅₀ parameterization presented in this work; MG: a₃₅₀ parameterization presented in Morel
 4 and Gentili (2009); P: a₃₅₀ parameterization presented in Preiswerk et al. (2000).

Study	Method		Annual flux (GgS yr ⁻¹)
Interpolation of observations			
Chin and Davis (1993)	sea surface OCS supersaturation ratios ^a		200 to 900
Watts (2000)	OCS surface concentration ^b		300*
Forward modeling			
	AQY/a₃₅₀	hydrolysis constant	
Kettle et al. (2002) ^c	AQY	Elliott et al., 1989	40**
Berry et al. (2013) ^d	from Kettle et al. (2002)	from Kettle et al. (2002)	736
This work standard run	a ₃₅₀ from MG	Elliott et al. (1989)	813

5 ^asea surface OCS supersaturation ratios from open oceans, upwelling zones and coastal
 6 regions

7 ^bOCS surface concentration from estuarine, coastal and open ocean environments

8 ^cBased on UV irradiance and apparent quantum yields from the literature. Lowest and highest
 9 boundaries of the estimates correspond to the lowest and highest AQY used.

10 ^d136 GgS yr⁻¹ taken from Kettle upper estimate. Added source of 600 GgS yr⁻¹ necessary to
 11 equilibrate the global budget.

12 * 100 GgS yr⁻¹ from open ocean and 200 GgS yr⁻¹ from coastal shores

13 ** uncertainty range: between -110 GgS yr⁻¹ and +190 GgS yr⁻¹

14
 15
 16
 17
 18
 19
 20

